

Mott Criticality as the Confinement Transition of a Pseudogap-Mott Metal

Abhirup Mukherjee,^{1,*} S. R. Hassan,^{2,†} Anamitra Mukherjee,^{3,‡}
N. S. Vidhyadhiraja,^{4,§} A. Taraphder,^{5,¶} and Siddhartha Lal^{1,**}

¹*Department of Physical Sciences, Indian Institute of Science Education and Research Kolkata, Nadia - 741246, India*

²*The Institute of Mathematical Sciences, HBNI, C.I.T. Campus, Chennai 600 113, India*

³*School of Physical Sciences, National Institute of Science, Education and Research, HBNI, Jatni 752050, India*

⁴*Theoretical Sciences Unit, Jawaharlal Nehru Center for Advanced Scientific Research, Jakkur, Bengaluru 560064, India*

⁵*Department of Physics, Indian Institute of Technology Kharagpur, Kharagpur 721302, India*

(Dated: November 4, 2025)

The phenomenon of Mott insulation involves the localization of itinerant electrons due to strong local repulsion. Upon doping, a pseudogap (PG) phase emerges - marked by selective gapping of the Fermi surface without conventional symmetry breaking in spin or charge channels. A key challenge is understanding how quasiparticle breakdown in the Fermi liquid gives rise to this enigmatic state, and how it connects to both the Mott insulating and superconducting phases. Here, we develop a renormalization-based construction of strongly correlated lattice models that captures the emergence of the pseudogap phase and its transition to a Mott insulator. Applying a many-body tiling scheme to the fixed-point impurity model uncovers a lattice model with electron interactions and Kondo physics. At half-filling, the interplay between Kondo screening and bath charge fluctuations in the impurity model leads to Fermi liquid breakdown. This reveals a pseudogap phase characterized by a non-Fermi liquid (the Mott metal) residing on nodal arcs, gapped antinodal regions of the Fermi surface, and an anomalous scaling of the electronic scattering rate with frequency. The eventual confinement of holon-doublon excitations of this exotic metal obtains a continuous transition into the Mott insulator. Our results identify the pseudogap as a distinct long-range entangled quantum phase, and offer a new route to Mott criticality beyond the paradigm of local quantum criticality.

I. INTRODUCTION

The Landau quasiparticle paradigm [1] underpins our understanding of metallic behaviour, where the screening of long-ranged repulsive interactions between delocalised electrons leads to well-defined excitations that carry the same quantum numbers as free electrons. This remarkable phenomenon - known as adiabatic continuity - is captured by excitations described by poles of the single-particle Greens function of the interacting system. But what defines metallicity when quasiparticles are no longer well-defined [2]? Can a surface of zeros of the Greens function [3], rather than poles forming a Fermi surface, define an entirely new kind of metal? Could such an exotic state serve as the precursor to Mott localisation driven purely by repulsion, and without invoking magnetic order [4]? These questions necessitate a radical departure in understanding conduction in correlated electron systems beyond the quasiparticle paradigm [5].

The anomalous pseudogap (PG) phase, observed in the cuprates, exhibits nodal-antinodal dichotomy with

spectral weight concentrated on Fermi arcs around the nodal regions [6–8]. In the PG phase of such Mott systems [9–38], the single-particle Green's function develops surfaces of zeros, also known as Luttinger surfaces [3, 39], that signals a fundamental obstruction to quasiparticle formation. As interaction strength increases, these zero surfaces proliferate, fragmenting the Fermi surface into nodal arcs [18, 39], violating the Luttinger sum rule by reconfiguring Fermi volume [40], and breaking an emergent \mathbb{Z}_2 symmetry associated with the conservation of spin currents in Fermi liquids [41, 42]. Unlike conventional instabilities driven by poles, this phenomenon marks a topological breakdown of Fermi liquid theory [2, 43]. We show that this breakdown arises from a strongly entangled, scale-invariant state of quantum matter, one that serves as the parent metal to the Mott insulator in a half-filled lattice model of strongly correlated electrons. This offers a concrete, controlled framework to understand both the non-quasiparticle character of the pseudogap phase and its continuous evolution into a repulsion-driven insulator, in full alignment with Mott's original vision [4].

Our approach involves developing a renormalization group (RG)-based impurity-to-lattice framework that reconstructs the low-energy physics of a strongly correlated system from the fixed-point structure of a quantum impurity model (Fig. 1(a)). Starting from a dynamical Anderson impurity embedded in a correlated bath, we solve the system using a unitary RG (URG) approach [44, 45]. We then construct a translation-invariant

* am18ip014@iiserkol.ac.in

† shassan@imsc.res.in

‡ anamitra@niser.ac.in

§ raja@jncasr.ac.in

¶ arghya@phy.iitkgp.ac.in

** slal@iiserkol.ac.in

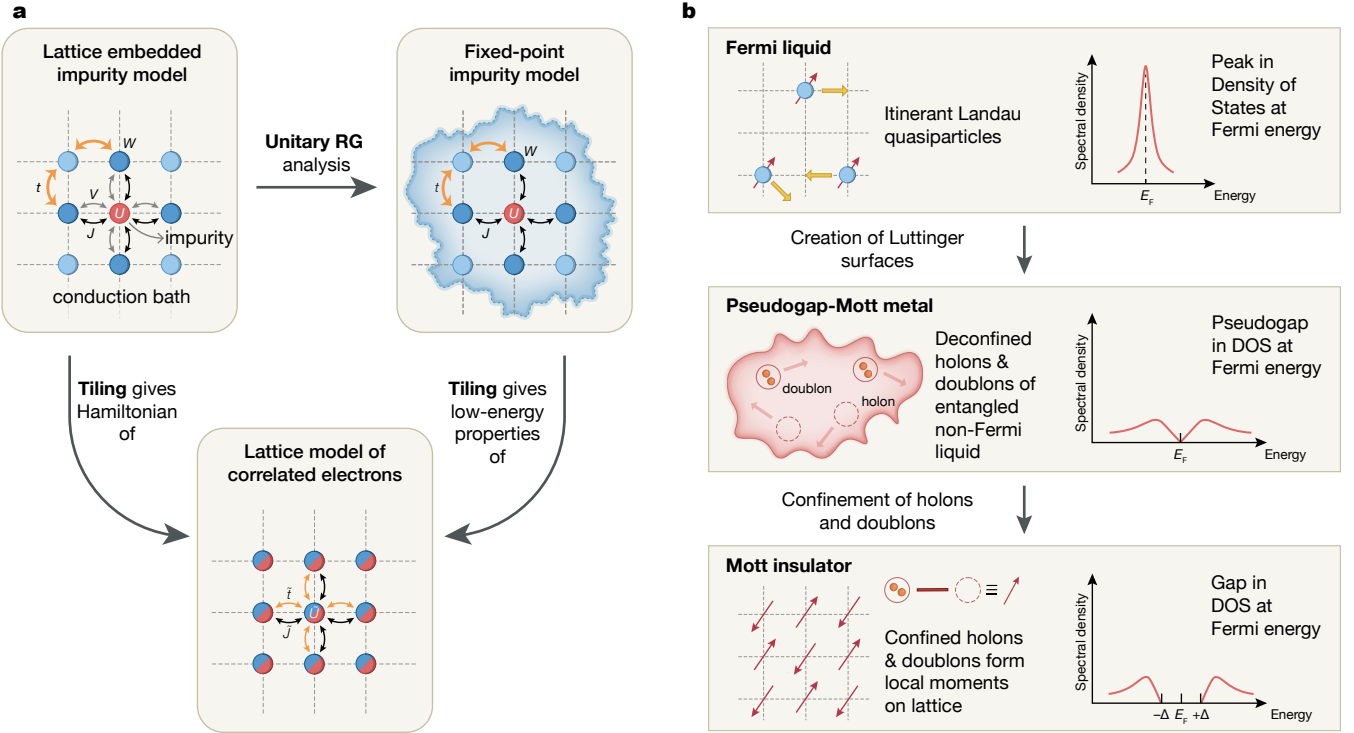


FIG. 1. Schematic representation of (a) theoretical framework adopted by us (see main text for explanation of symbols), (b) phases obtained for the extended Hubbard model in two dimensions at $T = 0$, and passage between them.

lattice Hamiltonian through a many-body tiling procedure that preserves non-local correlations and inherits momentum-resolved self-energies and renormalized couplings from the impurity solution. The resulting model is an *extended*-Hubbard Hamiltonian on a two-dimensional square lattice at half-filling, with both on-site repulsion and nearest-neighbour spin exchange interactions. These correlations, derived directly from the impurity dynamics, enable tracking the evolution from the FL to the Mott insulator (MI) via an intermediate PG phase.

A central insight of our work is that the PG phase hosts a NFL state governed by Kondo frustration and doublon–holon deconfinement [46] (Fig. 1(b)). A correlation scale (W) in the conduction bath suppresses Kondo screening (with coupling J) beyond a critical ratio of W/J , triggering the emergence of Luttinger surfaces in the lattice model. This breakdown of quasiparticles begins at the antinodes and progressively engulfs the nodal regions, driving a continuous transformation into the MI. The resulting NFL exhibits a pseudogapped density of states that vanishes as ω^2 as $\omega \rightarrow 0$, multipartite long-range entanglement, and a universal scattering rate of the form $\sim (a + b\omega^2)^{-1}$ that grows as $\omega \rightarrow 0$. At the critical endpoint of this phase, the URG flow identifies a singular NFL described by the Hatsugai–Kohmoto (HK) model [42, 47, 48], with fully deconfined holon–doublon excitations.

The emergence of Luttinger surfaces alters the anomaly structure associated with the generalized sym-

metry of the FS [49–51]. The corresponding topological charge is defined via the Luttinger–Ward functional. This charge is modified by Green’s function zeros, signalling a shift in the underlying anomaly. Within our framework, this reorganization grants topological protection to the RG flows terminating in the PG regime, ensuring the stability of its NFL excitations. These are adiabatically connected to the Hatsugai–Kohmoto model [47, 48], reinforcing the interpretation of the PG as a distinct quantum phase. We thus identify the NFL state as a new gapless, long-range entangled phase of correlated matter – the *Mott metal* – whose deconfined holon–doublon excitations are eventually confined across the Mott transition [4].

While we demonstrate our approach for an extended Hubbard model, the underlying framework is broadly applicable to correlated quantum systems. The impurity-plus-tiling construction accommodates multi-orbital degrees of freedom, frustrated geometries, and nontrivial band topology. By deriving lattice Hamiltonians directly from renormalized local dynamics – without relying on mean-field approximations – this method preserves non-local correlations and enhances momentum-space resolution. It thus provides a versatile and controlled route for engineering strongly correlated models, particularly in regimes where PG formation, NFL scaling, and Mott physics intersect.

We now describe the layout of the work. In section II, we formulate the lattice-embedded auxiliary quantum

impurity model and sketch the unitary renormalisation group (URG) method employed to analyse the impurity model. In section III, we formulate the tiling procedure by which to map the impurity Hamiltonian, eigenstates and observables into a lattice model of strongly correlated electrons via the usage of many-body translation operators. Section IV displays the destruction of the Fermi liquid from the breakdown of Kondo screening, leading to a pseudogapped non-Fermi liquid phase of matter. The novel properties of this phase are rigorously established in section V. In section VI, we demonstrate that the continuous transition between the pseudogap and Mott insulating phases is described by the exactly solvable Hatsugai-Kohmoto model. We demonstrate in section VII the universal organising principle that is responsible for the emergence of the pseudogap non-Fermi liquid phase. This also unveils the pseudogap as the strongly coupled long-range entangled parent metal of the Mott insulator. We conclude in section VIII. Finally, we present appendices containing the derivation of the URG analysis of the impurity model, and the exactly solvable model at the critical point.

II. AUXILIARY MODEL AND URG ANALYSIS

To capture the interplay between Kondo physics and Mott localization, our approach relies on a two-dimensional auxiliary model consisting of an Anderson impurity embedded in a minimally-correlated bath, which we solve the system using a unitary RG (URG) approach [44, 45]. The impurity model and URG analysis are laid out in this section. In order to make contact with a lattice model, we construct a translation-invariant Hamiltonian from the impurity model through a many-body tiling procedure: this preserves non-local correlations, as well as allows for momentum-resolved self-energies and renormalized couplings generated from the impurity solution. For the impurity model chosen in this work, tiling results in an *extended*-Hubbard Hamiltonian on a two-dimensional square lattice at particle-hole symmetry (half-filling). The interaction terms within the lattice model are a result of analogous correlations present in the auxiliary model. This is laid out next in Section III.

A. Lattice-embedded Impurity Model

The auxiliary model consists of a correlated impurity site (with a double occupancy cost U) embedded within a correlated conduction bath defined on a square lattice (see Fig. 1(a)). The impurity site hybridises with the conduction bath sites adjacent to it through one-particle hybridisation V as well as a spin-exchange interaction J arising from fluctuations in local spin densities of the electrons. The conduction bath has minimal correlations in the form of a local correlation term W on the sites

that are adjacent to the impurity.

The Hamiltonian of the auxiliary model studied here is

$$\mathcal{H}_{\text{aux}} = H_{\text{imp}} + H_{\text{coup}} + H_{\text{cbath}}, \quad (1)$$

where the particle-hole symmetric impurity term is

$$H_{\text{imp}} = -\frac{U}{2} (\hat{n}_{d\uparrow} - \hat{n}_{d\downarrow})^2, \quad (2)$$

describing on-site Coulomb interactions at the impurity. Here, $c_{d\sigma}^\dagger$ creates an electron with spin σ at the impurity site, and $\hat{n}_{d\sigma} = c_{d\sigma}^\dagger c_{d\sigma}$ denotes the corresponding number operator.

The impurity couples to four nearest-neighbour bath sites $c_{Z\sigma}$ through both hybridization and Kondo exchange:

$$H_{\text{coup}} = \frac{J}{2} \sum_{\sigma_1, \sigma_2, Z} \mathbf{S}_d \cdot c_{Z\sigma_1}^\dagger \boldsymbol{\tau}_{\sigma_1 \sigma_2} c_{Z\sigma_2} - V \sum_{\sigma, Z} (c_{Z\sigma}^\dagger c_{d\sigma} + \text{h.c.}), \quad (3)$$

where $\boldsymbol{\tau}$ are the Pauli matrices, and Z indexes the four neighbouring bath sites. The half-filled bath includes nearest neighbour hopping and on-site correlations on the site neighbouring the impurity:

$$H_{\text{cbath}} = \sum_{\mathbf{k}} \epsilon_{\mathbf{k}} c_{\mathbf{k},\sigma}^\dagger c_{\mathbf{k},\sigma} - \frac{W}{2} \sum_Z (\hat{n}_{Z\uparrow} - \hat{n}_{Z\downarrow})^2, \quad (4)$$

where $\epsilon_{\mathbf{k}} = -2t(\cos k_x + \cos k_y)$, and W parametrizes local repulsion in the bath that frustrates Kondo screening and drives the system towards local-moment formation. A crucial feature of this construction is that the Kondo coupling acquires a momentum structure upon Fourier transforming:

$$J_{\mathbf{k},\mathbf{k}'} = \frac{J}{2} [\cos(k_x - k'_x) + \cos(k_y - k'_y)], \quad (5)$$

which respects the C_4 symmetry of the square lattice.

B. The unitary renormalisation group method

In order to obtain the various low-energy phases of our impurity model, we perform a scaling analysis of the associated Hamiltonian using the recently developed unitary renormalisation group (URG) method [19, 39, 40]. The method has been applied successfully on a wide variety of problems of correlated fermions [52–57]. The method proceeds by resolving quantum fluctuations in high-energy degrees of freedom, leading to a low-energy Hamiltonian with renormalised couplings and new emergent degrees of freedom. Typically, for a system with Fermi energy ϵ_F and bandwidth E_N , the sequence of isoenergetic shells $\{E_{(j)}\}, E_j \in [E_0, E_N]$ define the states whose quantum fluctuations we sequentially resolve. The momentum states lying on shells E_N that are

far away from the Fermi surface comprise the UV states, while those on shells near the Fermi surface comprise the IR states.

As a result of the URG transformations, the Hamiltonian $H_{(j)}$ at a given RG step j involves scattering processes between the k -states that have energies lower than $D_{(j+1)}$. The unitary transformation $U_{(j)}$ is then defined so as to remove the number fluctuations of the currently most energetic set of states $D_{(j)}$ [44, 45]:

$$H_{(j-1)} = U_{(j)} H_{(j)} U_{(j)}^\dagger, \text{ such that } [H_{(j-1)}, \hat{n}_j] = 0. \quad (6)$$

The eigenvalue of \hat{n}_j has, thus, been rendered an integral of motion (IOM) under the RG transformation.

The unitary transformations can be expressed in terms of a generator $\eta_{(j)}$ that has fermionic algebra [44, 45]:

$$U_{(j)} = \frac{1}{\sqrt{2}} \left(1 + \eta_{(j)} - \eta_{(j)}^\dagger \right), \quad \{\eta_{(j)}, \eta_{(j)}^\dagger\} = 1, \quad (7)$$

where $\{\cdot\}$ is the anticommutator. The unitary operator $U_{(j)}$ that appears in Eq. (7) can be cast into the well-known general form $U = e^S, S = \frac{\pi}{4} (\eta_{(j)}^\dagger - \eta_{(j)})$ that a unitary operator can take, defined by an anti-Hermitian operator S . The generator $\eta_{(j)}$ is given by the expression[44, 45]

$$\eta_{(j)}^\dagger = \frac{1}{\hat{\omega}_{(j)} - \text{Tr}(H_{(j)} \hat{n}_j)} c_j^\dagger \text{Tr}(H_{(j)} c_j). \quad (8)$$

The operators $\eta_{(j)}, \eta_{(j)}^\dagger$ behave as the many-particle analogues of the single-particle field operators c_j, c_j^\dagger - they change the occupation number of the single-particle Fock space $|n_j\rangle$. The important operator $\hat{\omega}_{(j)}$ originates from the quantum fluctuations that exist in the problem because of the non-commutation of the kinetic energy terms and the interaction terms in the Hamiltonian:

$$\hat{\omega}_{(j)} = H_{(j-1)} - H_{(j)}^i. \quad (9)$$

$H_{(j)}^i$ is the part of $H_{(j)}$ that commutes with \hat{n}_j but does *not* commute with at least one \hat{n}_l for $l < j$. The RG flow continues up to energy D^* , where a fixed point is reached from the vanishing of the RG function. Detailed comparisons of the URG with other methods (e.g., the functional RG, spectrum bifurcation RG etc.) can be found in Refs. [44, 54], and implementation on the present problem in Appendix A.

III. TILING FORMALISM

A. Reconstructing of lattice model from auxiliary model

To reconstruct a translationally invariant lattice Hamiltonian from the impurity model (with Hamiltonian

\mathcal{H}_{aux}), we define a many-body tiling prescription that embeds the auxiliary impurity system uniformly across the two-dimensional square lattice. Thus, the tiling process systematically derives the full lattice dynamics from the renormalized fixed-point structure of the impurity. As described in Section II, the auxiliary model consists of a single impurity embedded in a correlated bath at the location \mathbf{r}_d :

$$H(\mathbf{r}_d) = H_{\text{imp}} + H_{\text{cbath}} + H_{\text{imp-cbath}}. \quad (10)$$

The form of various terms in eq.(10) have been defined in eqs.(2), (3) and (4) in Section II.

The tiled lattice Hamiltonian is generated by symmetrically translating this impurity model:

$$\mathcal{H}_{\text{tiled}} = \mathcal{T}[H(\mathbf{r}_d)] = \sum_{\mathbf{r}} T^\dagger(\mathbf{r} - \mathbf{r}_d) H(\mathbf{r}_d) T(\mathbf{r} - \mathbf{r}_d), \quad (11)$$

where $T(\mathbf{a})$ are many-body translation operators [58]:

$$T^\dagger(\mathbf{a}) \mathcal{O}(\{\mathbf{r}_i\}) T(\mathbf{a}) = \mathcal{O}(\{\mathbf{r}_i + \mathbf{a}\}). \quad (12)$$

Applying this to each term yields:

$$\begin{aligned} \mathcal{T}[H_{\text{cbath}}] &= -\frac{(N-2)t}{\sqrt{\mathcal{Z}}} \sum_{\langle \mathbf{r}_i, \mathbf{r}_j \rangle; \sigma} (c_{\mathbf{r}_i \sigma}^\dagger c_{\mathbf{r}_j \sigma} + \text{h.c.}) \\ &\quad - \frac{1}{2} W \sum_{\mathbf{r}} (\hat{n}_{\mathbf{r}\uparrow} - \hat{n}_{\mathbf{r}\downarrow})^2, \\ \mathcal{T}[H_{\text{imp}}] &= -\frac{U}{2} \sum_{\mathbf{r}} (\hat{n}_{\mathbf{r}\uparrow} - \hat{n}_{\mathbf{r}\downarrow})^2, \\ \mathcal{T}[H_{\text{imp-cbath}}] &= \sum_{\langle \mathbf{r}_i, \mathbf{r}_j \rangle} \left[\frac{2J}{\mathcal{Z}} \mathbf{S}_{\mathbf{r}_i} \cdot \mathbf{S}_{\mathbf{r}_j} - \frac{2V}{\sqrt{\mathcal{Z}}} \sum_{\sigma} (c_{\mathbf{r}_i \sigma}^\dagger c_{\mathbf{r}_j \sigma} + \text{h.c.}) \right], \end{aligned} \quad (13)$$

with local spin operators defined as

$$\mathbf{S}_{\mathbf{r}} = \sum_{\sigma, \sigma'} c_{\mathbf{r} \sigma}^\dagger \boldsymbol{\tau}_{\sigma \sigma'} c_{\mathbf{r} \sigma'}. \quad (14)$$

To avoid overcounting of the non-interacting bath terms, we subtract extra copies of the kinetic energy term. The reconstructed extended–Hubbard model then reads:

$$\begin{aligned} \mathcal{H}_{\text{tiled}} &= -\frac{1}{\sqrt{\mathcal{Z}}} \tilde{t} \sum_{\langle \mathbf{r}_i, \mathbf{r}_j \rangle; \sigma} (c_{\mathbf{r}_i \sigma}^\dagger c_{\mathbf{r}_j \sigma} + \text{h.c.}) \\ &\quad + \frac{\tilde{J}}{\mathcal{Z}} \sum_{\langle \mathbf{r}_i, \mathbf{r}_j \rangle} \mathbf{S}_{\mathbf{r}_i} \cdot \mathbf{S}_{\mathbf{r}_j} - \frac{1}{2} \tilde{U} \sum_{\mathbf{r}} (\hat{n}_{\mathbf{r}\uparrow} - \hat{n}_{\mathbf{r}\downarrow})^2, \end{aligned} \quad (15)$$

where the effective lattice couplings are given by:

$$\tilde{t} = t + 2V, \quad \tilde{U} = U + W, \quad \tilde{J} = 2J. \quad (16)$$

A non-zero chemical potential in the bath and/or the impurity can be included to study the effects of doping. Crucially, the eigenstates of $\mathcal{H}_{\text{tiled}}$ obey a many-body generalization of Bloch’s theorem [58], which allows

for the exact computation of momentum-resolved observables (presented here for a 77×77 \mathbf{k} -space Brillouin zone grid). We shall demonstrate below that the lattice embedding and tiling procedures provide a controlled route to capture low-energy NFL behavior and Mott criticality directly from a quantum impurity model.

B. Mapping eigenstates using a many-body Bloch's theorem

As mentioned above, the eigenstates $|\Psi_s\rangle$ ($s = (\mathbf{k}, n)$) of the lattice Hamiltonians obtained using the tiling procedure enjoy a *many-body* Bloch's theorem [58], as the tiling procedure restores the translation symmetry of the Hamiltonian. This means that the *local* eigenstates $|\psi_n(\mathbf{r}_d)\rangle$ (with the impurity located at an arbitrary position \mathbf{r}_d) of the unit cell auxiliary model Hamiltonian $\mathcal{H}_{\text{aux}}(\mathbf{r}_d)$ can be used to construct eigenstates of the lattice Hamiltonian. The index $n (= 0, 1, \dots)$ in the subscript indicates that it is the n^{th} eigenstate of the auxiliary model.

The state $|\psi_n(\mathbf{r}_d)\rangle$ does not specify the position of the zeroth site, because the unit cell Hamiltonian $\mathcal{H}_{\text{aux}}(\mathbf{r}_d)$ itself has been averaged over \mathcal{Z} zeroth sites. Accordingly, we can express the averaged eigenstate $|\psi_n(\mathbf{r}_d)\rangle$ as

$$|\psi_n(\mathbf{r}_d)\rangle = \frac{1}{\sqrt{\mathcal{Z}}} \sum_{\mathbf{z} \in \text{NN}(\mathbf{r}_d)} |\psi_n(\mathbf{r}_d, \mathbf{z})\rangle , \quad (17)$$

where $|\psi_n(\mathbf{r}_d, \mathbf{z})\rangle$ is an auxiliary model eigenstate with the impurity and zeroth sites placed at \mathbf{r}_d and \mathbf{z} . With this in mind, the following unnormalised combination of the auxiliary model eigenstates satisfies a many-particle equivalent of Bloch's theorem [53]:

$$|\Psi_s\rangle \equiv |\Psi_{\mathbf{k}, n}\rangle = \frac{1}{\sqrt{N}} \sum_{\mathbf{r}_d} e^{i\mathbf{k} \cdot \mathbf{r}_d} |\psi_n(\mathbf{r}_d)\rangle \quad (18)$$

where N is the total number of lattice sites and \mathbf{r}_d is summed over all lattice spacings. The set of $n = 0$ states form the lowest band in the spectrum of the lattice, while higher values of n produce the more energetic bands. The ground state $s = s_0$ is obtained by setting \mathbf{k} and n to 0:

$$|\Psi_{\text{gs}}\rangle = \frac{1}{\sqrt{N}} \sum_{\mathbf{r}_d} e^{i\mathbf{k} \cdot \mathbf{r}_d} |\psi_{\text{gs}}(\mathbf{r}_d)\rangle \quad (19)$$

C. Mapping the retarded Greens function from auxiliary model to lattice model

We now show how to relate the one-particle retarded Greens functions of the bulk lattice to that of the auxiliary model. The retarded time-domain lattice k -space Greens function is defined as

$$\tilde{G}(\mathbf{K}\sigma; t) = -i\theta(t) \langle \Psi_{\text{gs}} | \{c_{\mathbf{K}\sigma}(t), c_{\mathbf{K}\sigma}^\dagger\} | \Psi_{\text{gs}} \rangle . \quad (20)$$

where the bulk Hamiltonian H_{tiled} leads to the dynamics of the annihilation operators at time t :

$$c_{\mathbf{K}\sigma}(t) = e^{itH_{\text{tiled}}} c_{\mathbf{K}\sigma} e^{-itH_{\text{tiled}}} . \quad (21)$$

We now proceed to simplify one of the terms of the anti-commutator (for simplicity of notation):

$$\begin{aligned} & \langle \Psi_{\text{gs}} | c_{\mathbf{K}\sigma}(t) c_{\mathbf{K}\sigma}^\dagger | \Psi_{\text{gs}} \rangle \\ &= \frac{1}{N^2} \sum_{\vec{r}, \vec{\Delta}} e^{-i\mathbf{K}_0 \cdot \vec{\Delta}} \langle \psi_0(\vec{r} + \vec{\Delta}) | c_{\mathbf{K}\sigma}(t) c_{\mathbf{K}\sigma}^\dagger | \psi_0(\vec{r}) \rangle . \end{aligned} \quad (22)$$

Using eq. (18), eq. (22) becomes

$$\langle \Psi_{\text{gs}} | c_{\mathbf{K}\sigma}(t) c_{\mathbf{K}\sigma}^\dagger | \Psi_{\text{gs}} \rangle = \frac{1}{N^2} \sum_s \sum_{\vec{r}, \vec{\Delta}} \sum_{\vec{r}', \vec{\Delta}'} e^{-i\vec{k}_0 \cdot \vec{\Delta}} e^{i\vec{k} \cdot \vec{\Delta}'} \langle \psi_0(\vec{r} + \vec{\Delta}) | c_{\mathbf{K}\sigma}(t) | \psi_n(\vec{r}' + \vec{\Delta}') \rangle \langle \psi_n(\vec{r}') | c_{\mathbf{K}\sigma}^\dagger | \psi_0(\vec{r}) \rangle . \quad (23)$$

In order to bring this expression closer to the form of an auxiliary model Greens function, we

- use the relation $|\psi(\vec{r} + \Delta)\rangle = T^\dagger(\vec{\Delta}) |\psi(\vec{r})\rangle$, where $T^\dagger(\vec{\Delta})$ translates all lattice sites by the vector $\vec{\Delta}$,
- use the property $T(\vec{a}) c(\mathbf{K}) T^\dagger(\vec{a}) = e^{-i\mathbf{K} \cdot \vec{a}} c(\mathbf{K})$, and
- make the substitution $\vec{\Delta}' \rightarrow \vec{\Delta}' + \vec{\Delta}$.

This leads to the expression

$$\langle \Psi_{\text{gs}} | c_{\mathbf{K}\sigma}(t) c_{\mathbf{K}\sigma}^\dagger | \Psi_{\text{gs}} \rangle = \frac{1}{N} \sum_n \sum_{\vec{r}, \vec{r}', \vec{\Delta}'} e^{i(\vec{k}_0 + \mathbf{K}) \cdot \vec{\Delta}'} \langle \psi_0(\vec{r}) | c_{\mathbf{K}\sigma}(t) | \psi_n(\vec{r}' + \vec{\Delta}') \rangle \langle \psi_n(\vec{r}') | c_{\mathbf{K}\sigma}^\dagger | \psi_0(\vec{r}) \rangle , \quad (24)$$

where the sum over $s = (\vec{k}, n)$ has been reduced to a sum over the auxiliary model eigenstate index n because of the Kronecker delta $\delta(\vec{k}_0 + \mathbf{K} - \vec{k})$. This can be further simplified by splitting the sum over $\vec{\Delta}'$ into positive and

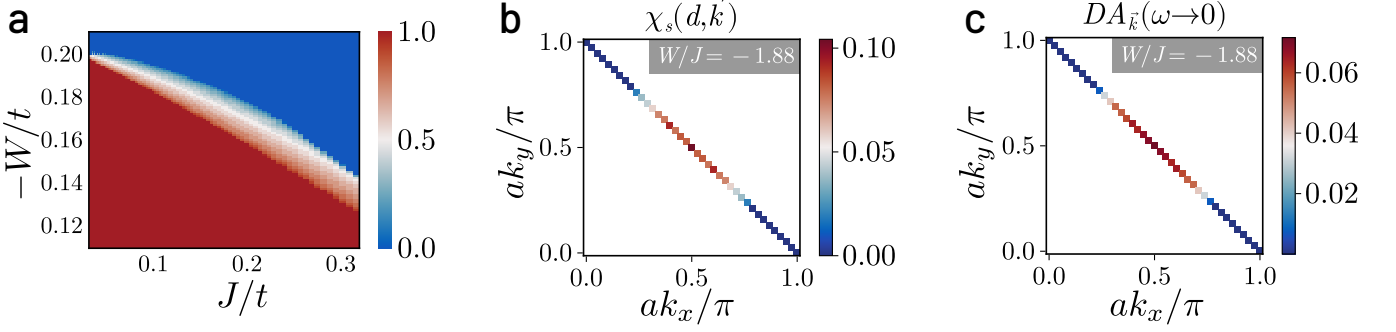


FIG. 2. (a) Phase diagram of impurity model at strong coupling in U in terms of competing dimensionless Kondo (J/t) and bath correlation (W/t) couplings. Colourbar represents the fraction of states on the Fermi surface replaced by zeros of the Greens function (Luttinger surface). A pseudogap phase (shaded region) is observed between the local Fermi liquid (red region) and local moment (blue region) phases (b) k -space-resolved spin-spin correlation $\chi_s(d, \mathbf{k}) = \langle \mathbf{S}_d \cdot \mathbf{S}_k \rangle$ in the pseudogap phase of the impurity model. Antinodal regions are observed to decouple from Kondo screening of the impurity. (c) Upon tiling, this leads to a k -space-resolved antinodal gap in the electronic density of states of the lattice model, corresponding to Luttinger surfaces of zeros.

negative parts and then making the transformation $\vec{r}' \rightarrow \vec{r}' + \vec{\Delta}'$:

$$\begin{aligned} \sum_{\vec{r}', \vec{\Delta}'} e^{i(\vec{k}_0 + \mathbf{K}) \cdot \vec{\Delta}'} |\psi_n(\vec{r}' + \vec{\Delta}')\rangle \langle \psi_n(\vec{r}')| &= \frac{1}{2} \sum_{\vec{r}', \vec{\Delta}'} \left[e^{i(\vec{k}_0 + \mathbf{K}) \cdot \vec{\Delta}'} |\psi_n(\vec{r}' + \vec{\Delta}')\rangle \langle \psi_n(\vec{r}')| + e^{-i(\vec{k}_0 + \mathbf{K}) \cdot \vec{\Delta}'} |\psi_n(\vec{r}' - \vec{\Delta}')\rangle \langle \psi_n(\vec{r}')| \right], \\ &= \frac{1}{2} \sum_{\vec{r}', \vec{\Delta}'} \left[e^{i(\vec{k}_0 + \mathbf{K}) \cdot \vec{\Delta}'} |\psi_n(\vec{r}' + \vec{\Delta}')\rangle \langle \psi_n(\vec{r}')| + e^{-i(\vec{k}_0 + \mathbf{K}) \cdot \vec{\Delta}'} |\psi_n(\vec{r}')\rangle \langle \psi_n(\vec{r}' + \vec{\Delta}')| \right]. \end{aligned} \quad (25)$$

For each pair of \vec{r}' and $\vec{\Delta}'$, the term within the box brackets has the form of a two-level Hamiltonian between the states $|\psi_n(\vec{r}')\rangle$ and $|\psi_n(\vec{r}' + \vec{\Delta}')\rangle$, with a tunnelling amplitude $e^{i(\vec{k}_0 + \mathbf{K}) \cdot \vec{\Delta}'}$. The term can therefore be written in the eigenbasis of this Hamiltonian:

$$\sum_{\vec{r}', \vec{\Delta}'} e^{i(\vec{k}_0 + \mathbf{K}) \cdot \vec{\Delta}'} |\psi_n(\vec{r}' + \vec{\Delta}')\rangle \langle \psi_n(\vec{r}')| = \frac{1}{2} \sum_{\vec{r}', \vec{\Delta}'} \left[|\chi_n^+(\vec{r}', \vec{\Delta}')\rangle \langle \chi_n^+(\vec{r}', \vec{\Delta}')| - |\chi_n^-(\vec{r}', \vec{\Delta}')\rangle \langle \chi_n^-(\vec{r}', \vec{\Delta}')| \right], \quad (26)$$

where $|\chi_n^\pm(\vec{r}', \vec{\Delta}')\rangle = \frac{1}{\sqrt{2}} \left[|\psi_n(\vec{r}')\rangle \pm e^{i(\vec{k}_0 + \mathbf{K}) \cdot \vec{\Delta}'} |\psi_n(\vec{r}' + \vec{\Delta}')\rangle \right]$ are the eigenvectors of the tunnelling Hamiltonian with eigenvalues ± 1 respectively. With this basis transformation, we can rewrite eq. (24) as

$$\langle \Psi_{\text{gs}} | c_{\mathbf{K}\sigma}(t) c_{\mathbf{K}\sigma}^\dagger | \Psi_{\text{gs}} \rangle = \frac{1}{2N} \sum_n \sum_{\vec{r}, \vec{r}', \vec{\Delta}'} \langle \psi_0(\vec{r}) | c_{\mathbf{K}\sigma}(t) \left[|\chi_n^+(\vec{r}', \vec{\Delta}')\rangle \langle \chi_n^+(\vec{r}', \vec{\Delta}')| - |\chi_n^-(\vec{r}', \vec{\Delta}')\rangle \langle \chi_n^-(\vec{r}', \vec{\Delta}')| \right] c_{\mathbf{K}\sigma}^\dagger | \psi_0(\vec{r}) \rangle. \quad (27)$$

In the present work, we consider only the $\vec{r}' = \vec{r}$, $\vec{\Delta}' = 0$ component. These terms represent those contributions to the total Greens function that arise from excitations that start and end at a specific auxiliary model (at \vec{r}), and also evolve dynamically within the same auxiliary model. These terms are therefore exactly equal to the auxiliary model Greens function at position \vec{r} , and are the most dominant contribution due to the localised nature of the impurity model. Thus, restricting ourselves to just the

single auxiliary model contributions gives

$$\begin{aligned} \langle \Psi_{\text{gs}} | c_{\mathbf{K}\sigma}(t) c_{\mathbf{K}\sigma}^\dagger | \Psi_{\text{gs}} \rangle &= \\ \frac{1}{N} \sum_{n, \vec{r}} \langle \psi_0(\vec{r}) | c_{\mathbf{K}\sigma}(t) | \psi_n(\vec{r}) \rangle \langle \psi_n(\vec{r}) | c_{\mathbf{K}\sigma}^\dagger | \psi_0(\vec{r}) \rangle. \end{aligned} \quad (28)$$

We now consider more carefully the transition operator $\mathcal{T}_{\mathbf{K}\sigma} = c_{\mathbf{K}\sigma}$ for the 1-particle excitation giving rise to the above Greens function. Within our auxiliary model approach, gapless excitations within the lattice model are represented by gapless excitations of the impurity site, specifically those that screen the impurity site and form the local Fermi liquid. As a result, the uncoordinated

\mathcal{T} -matrix for the lattice model must be replaced by a combined \mathcal{T} -matrix within the impurity model that captures those gapless excitations that occur in connection with the impurity, and projects out the uncorrelated excitations that take place even when the impurity site is decoupled from the bath.

In order to construct this auxiliary model \mathcal{T} -matrix, we note that the impurity site can have both spin and charge excitations. Considering both excitations, the modified \mathcal{T} -matrix that constructs k -space excitations in correlation with the impurity site are

$$\mathcal{T}_{\mathbf{K}\sigma} = c_{\mathbf{K}\sigma} \left(\sum_{\sigma'} c_{d\sigma}^\dagger + \text{h.c.} \right) + c_{\mathbf{K}\sigma} (S_d^+ + \text{h.c.}) , \quad (29)$$

leading to the updated expression for the complete Greens function:

$$\begin{aligned} \tilde{G}(\mathbf{K}\sigma; t) &= -\frac{i\theta(t)}{N} \sum_{n,\vec{r}} \langle \psi_0(\vec{r}) | [\mathcal{T}_{\mathbf{K}\sigma}(t) |\psi_n(\vec{r})\rangle \langle \psi_n(\vec{r})| \mathcal{T}_{\mathbf{K}\sigma}^\dagger \\ &\quad + \mathcal{T}_{\mathbf{K}\sigma}^\dagger |\psi_n(\vec{r})\rangle \langle \psi_n(\vec{r})| \mathcal{T}_{\mathbf{K}\sigma}(t)] | \psi_0(\vec{r}) \rangle . \end{aligned} \quad (30)$$

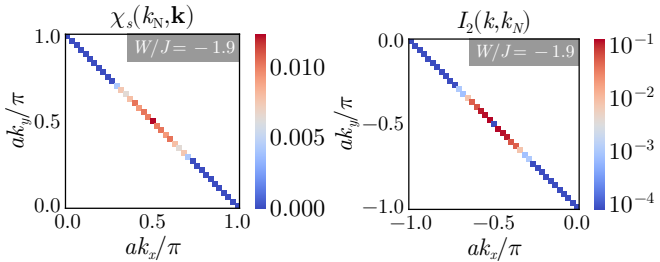


FIG. 3. Left: Spin correlations χ_s for the *tiled model*, between the nodal point $k_N = (-\pi/2, -\pi/2)$ and an arbitrary k -point on the Fermi surface. In the PG, the spin-correlations near the antinode vanish, indicating that they have been removed from the metallic excitations, while the correlations near the nodal point become enhanced because of the increasingly correlated nature of the metal. Right: Mutual information I_2 between an arbitrary k -state and the nodal point. The nodal points remain strongly entangled with each other all the way through the PG.

IV. PSEUDOGAP FORMATION VIA KONDO BREAKDOWN

A. RG Phase Diagram

A detailed picture of the PG in the impurity model is obtained from a momentum-resolved breakdown of Kondo screening in the strong-coupling regime $U \gg t$ phase of H_{aux} . A unitary renormalisation group (URG) scaling analysis [44] obtains a flow equation of the Kondo

coupling $J_{\mathbf{k}_1, \mathbf{k}_2}^{(j)}$ (see Appendix A for details)

$$\Delta J_{\mathbf{k}_1, \mathbf{k}_2}^{(j)} = - \sum_{\mathbf{q} \in \text{PS}} \frac{J_{\mathbf{k}_2, \mathbf{q}}^{(j)} J_{\mathbf{q}, \mathbf{k}_1}^{(j)} + 4J_{\mathbf{q}, \bar{\mathbf{q}}}^{(j)} W_{\bar{\mathbf{q}}, \mathbf{k}_2, \mathbf{k}_1, \mathbf{q}}}{\omega - \frac{1}{2}|\varepsilon_j| + J_{\mathbf{q}}^{(j)}/4 + W_{\mathbf{q}}/2} , \quad (31)$$

where ε_j is the energy of the shell being decoupled at the j^{th} step, the sum is over all occupied momentum states \mathbf{q} of the energy shell ε_j , and $\bar{\mathbf{q}} = \mathbf{q} + \boldsymbol{\pi}$ is the particle-hole transformed state associated with \mathbf{q} . The bath interaction coupling $W_{\bar{\mathbf{q}}, \mathbf{k}_2, \mathbf{k}_1, \mathbf{q}}$ is found to be marginal under these transformations. While we present a detailed numerical evaluation of the RG equation for $J_{\mathbf{k}_1, \mathbf{k}_2}$ (eq.(31)) below, it is clear that the frustration of Kondo screening due to charge fluctuations (for attractive bath interactions $W < 0$) leads to the Mott transition [59].

A detailed numerical computation of the URG equation in eq. (31) leads to the phase diagram shown in Fig. 2(a). Upon tuning the ratio of the bath and Kondo interactions (W/J) from zero to negative values, the following phases emerge in the impurity model from the competition between J and W in eq. (31): (i) for $W/J < (W/J)_{\text{PG}}$, an LFL phase (red region), where the entire FS participates in Kondo screening, (ii) for $\frac{W}{J} \in [(W/J)_{\text{PG}}, (W/J)_c]$ (shaded region), a local PG phase where disconnected parts of the FS around the node participate in Kondo screening, and (iii) a local moment phase for $\frac{W}{J} > (W/J)_c$ (blue region), where the impurity remains unscreened at low-energies. These can be visualised from spin correlations, $\chi_s(d, \mathbf{k}) = \langle \mathbf{S}_d \cdot \mathbf{S}_k \rangle$, as shown in Fig. 2(b) for the PG. The values $(W/J)_{\text{PG}}$ and $(W/J)_c$ are therefore the entry into and exit from the PG phase.

Mapping onto the lattice model via tiling, we observe that RG-induced nodal–antinodal dichotomy in $J_{\mathbf{k}, \mathbf{k}'}$ in the impurity model is the microscopic origin of the PG in the lattice model: the extinction of Kondo coherence translates into spectral zeros in the lattice Green’s function (i.e., Luttinger surfaces) at antinodal momenta (Fig. 2(c)). This establishes that the $T = 0$ Mott transition of the 2D *extended*-Hubbard model proceeds from FL to MI through an intervening PG phase. In Fig. 3, similar insights obtain from the spin-correlation $\chi_s(\mathbf{k}, k_N) = \langle \mathbf{S}_k \cdot \mathbf{S}_{k_N} \rangle$ in k -space (where k_N is the nodal momentum) and mutual information $I_2(\mathbf{k} : k_N)$ between two momentum states: the PG displays Fermi arcs in the nodal regions along with vanishing correlation and entanglement in the antinodal regions.

B. Unravelling of Kondo Screening

The \mathbf{k} -space anisotropy of Kondo breakdown can be visualized in terms of zeros of $J_{\mathbf{k}_N, \mathbf{k}}$, involving spin-flip scattering between the node $\mathbf{k}_N = (\pi/2, \pi/2)$ and a general wavevector \mathbf{k} . For any W/J , the C_4 lattice symmetry dictates that $J_{\mathbf{k}_N, \mathbf{k}}$ vanishes if \mathbf{k} belongs to any of the antinodes or adjacent nodes. Tuning W/J towards

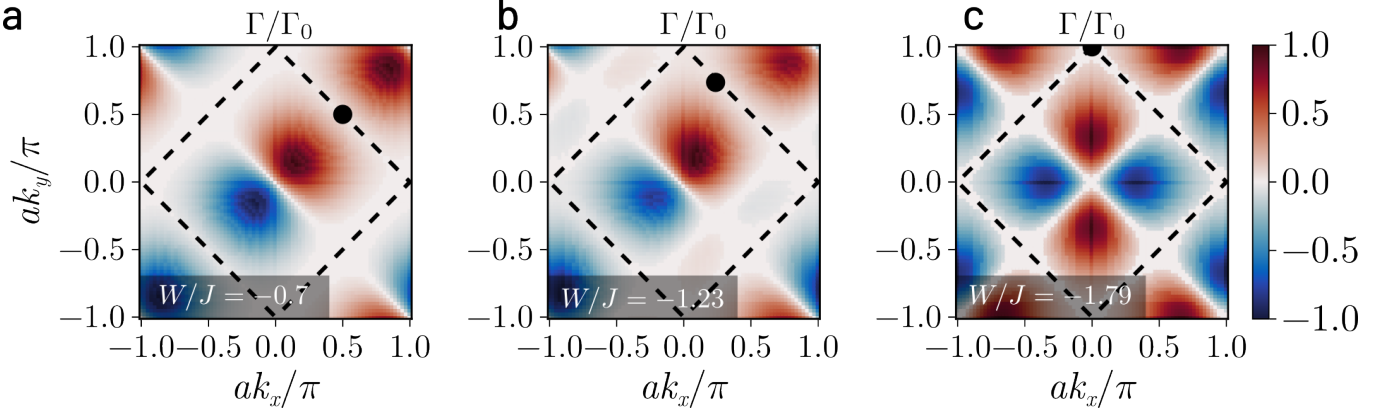


FIG. 4. Initiation of the decoupling of $J_{\mathbf{k},\mathbf{k}'}$ (positive, negative and zeros shown in red, blue and white respectively), with \mathbf{k} (black circle) at low-energies for \mathbf{k} corresponding to the node (a), antinode (b) and a point mid-way between them (c) on the top right arm of the FS respectively with tuning W/J . As dictated by the symmetry of $J_{\mathbf{k},\mathbf{k}'}$, the decoupling for a given \mathbf{k} proceeds via the appearance of zeros (white patches) of $J_{\mathbf{k},\mathbf{k}'}$ for \mathbf{k}' initially on the nodal regions of adjacent arms, and progresses gradually towards the antinodes. The decoupling ends with the onset of the pseudogap.

$(W/J)_{\text{PG}}$ leads to an unravelling of the Kondo screening: $J_{\mathbf{k}_N,\mathbf{k}}$ for \mathbf{k} close to the adjacent nodes turns RG-irrelevant first, and a patch of zeros subsequently appears in $J_{\mathbf{k}_N,\mathbf{k}}$ around this point (Fig. 4(a)). Tuning W/J further extends the patch of zeros towards the antinodes (Fig. 4(b) and 4(c)). Kondo screening thus unravels by a systematic decoupling of all $J_{\mathbf{k}_1,\mathbf{k}_2}$ that connect adjacent quadrants of the Brillouin zone.

Precisely at $W/J = (W/J)_{\text{PG}}$, the antinode joins this connected region of zeros in $J_{\mathbf{k}_1,\mathbf{k}_2}$, marking the decoupling of the antinodes from all other points in the neighbourhood of the FS. This is an interaction-driven Lifshitz transition of the FS, and marks the entry into a PG phase possessing Fermi arcs [60]. Importantly, it coincides with an emergent two-channel Kondo (2CK) impurity model, where each channel corresponds to a pair of Fermi arcs on opposite faces of the conduction bath FS. The 2CK nature of the PG is guaranteed by the symmetry of $J_{\mathbf{k},\mathbf{k}'}$:

$$J_{\mathbf{k},\mathbf{k}'} = -J_{\mathbf{k}+\mathbf{Q},\mathbf{k}'} = -J_{\mathbf{k},\mathbf{k}'+\mathbf{Q}}, \quad \mathbf{Q} = (\pi, \pi). \quad (32)$$

The PG expands by shrinking these disconnected Fermi arcs towards the respective nodes, leading to nodal metals whose disappearance heralds the Mott transition.

C. Momentum-resolved Dynamical Spectral Weight Transfer

Passage through the PG phase is accompanied by a highly structured transfer of spectral weight across the FS. Strong charge fluctuations develop between the nodal and antinodal regions of the FS in the PG regime of the impurity model (Fig. 5(a)), as captured by the correlator:

$$\chi_c(\mathbf{k}_1, \mathbf{k}_2) = \left\langle c_{\mathbf{k}_1\downarrow}^\dagger c_{\mathbf{k}_1\downarrow}^\dagger c_{\mathbf{k}_2\downarrow} c_{\mathbf{k}_2\downarrow} + \text{h.c.} \right\rangle. \quad (33)$$

These fluctuations dynamically redistribute low-energy spectral weight from the antinodes to higher energies,

leading to selective gap formation. Accordingly, the Luttinger surfaces of the PG [3] coincides with the appearance of poles of the lattice model self-energy $\Sigma(\mathbf{k}, \omega = 0)$ near the antinodes; these poles approach the nodes on tuning towards the Mott transition (Fig. 5(b)). This mirrors the coalescing of finite-frequency poles of the self-energy poles towards zero frequency in the underlying impurity model (Fig. 5(c)).

V. NON-FERMI LIQUID EXCITATIONS WITHIN THE PSEUDOGAP

A. Pseudogapped spectral function and singular self-energy

In the PG regime, the nature of gapless Fermi arcs changes dramatically. We have already argued that the low-energy dynamics of these gapless Fermi arcs are governed by an underlying two-channel Kondo (2CK) impurity model [61, 62]. This is consistent with the rapid fall of the impurity quasiparticle residue Z_{imp} (Fig. 6(a)) from finite values in the FL phase to vanishingly small values just before the onset of the PG. Inset shows the simultaneous emergence of increasingly uncompensated local magnetic moments upon traversing the PG phase. The accompanying impurity spectral function of the gapless arcs show a pseudogapped behaviour for $\omega \simeq 0$, with a rapid fall in the spectral weight at $\omega = 0$ upon traversing the PG (Fig. 6(c)). The collapse of the Kondo resonance into a pseudogapped spectral function is accompanied by the redistribution of spectral weight [3] in the impurity spectral function (Fig. 6(b)) from $\omega \sim 0$ to the Hubbard sidebands at finite frequencies $\omega \simeq \pm 3$ (in units of the bandwidth).

Concomitant with this is the emergence of a zero-frequency peak in the imaginary part of the self-energy

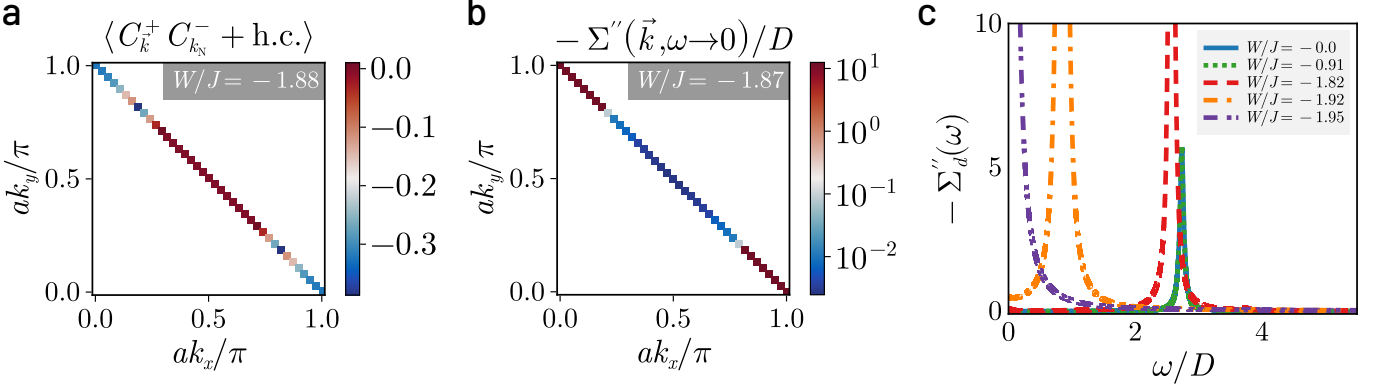


FIG. 5. (a) Enhanced charge correlations $\chi_c(\mathbf{k}_1, \mathbf{k}_2) = \langle c_{\mathbf{k}_1\uparrow}^\dagger c_{\mathbf{k}_1\downarrow}^\dagger c_{\mathbf{k}_2\downarrow} c_{\mathbf{k}_2\uparrow} + \text{h.c.} \rangle$ between the nodal and antinodal regions, signalling Kondo breakdown in the pseudogap phase of the impurity model. (b) In turn, the breakdown leads to the gapping of the antinodal regions in the lattice model, seen from the appearance of poles in the imaginary part of the self-energy. (c) The imaginary part of the impurity self-energy $\Sigma''(\omega > 0)$ possesses a pole at non-zero ω in the PG that moves towards $\omega = 0$ as the Mott transition is approached.

of the NFL in the PG phase(Fig. 7(a)),

$$-1/\Sigma''(\omega) \sim 1/\Sigma''(0) + \omega^\beta. \quad (34)$$

Remarkably, we find that the exponent $\beta = 2$ characterises the NFL for the entire PG phase (see Fig. 7(b)), including the critical end-point. This is in stark contrast with the $\Sigma''(\omega) \sim \omega^2$ for the FL (Fig. 7(b)). A similar analysis reveals the power-law scaling for the low-frequency behaviour of the impurity spectral function in Fig.8. We observe that $A_d(\omega) \sim A_d(0) + \omega^2$ for the pseudogap phase, while $1/A_d(\omega) \sim 1/A_d(0) + \omega^2$ for the Fermi liquid (inset of Fig. 8).

B. Finite-Frequency Scattering Rate and Optical Response Through the Pseudogap

All $\Sigma''(\omega)$ for the NFL are observed to lie above the Mott-Ioffe-Regel (MIR) bound [63, 64] (dashed blue line in Fig. 7(a)), while those for the FL lie below. The MIR bound is the maximum expected scattering rate in metals when the mean free path approaches the lattice spacing:

$$-2\Sigma''_{\text{MIR}} = 1/\tau_{\text{MIR}}, \quad \tau_{\text{MIR}} = l_{\min}/v_F, \quad (35)$$

where l_{\min} is the minimum mean free path in metals (equal to one lattice spacing) and τ_{MIR} is the associated lifetime of quasiparticles close to the FS (with Fermi velocity v_F). The height of the zero-frequency peak rises by almost 4 orders of magnitude from the start of the PG till its end at the Mott transition point (Fig. 7(c)); the dramatic growth of the peak height very near the Mott critical point coincides with the coalescing of the finite-frequency poles of the self-energy into a single pole at zero-frequency, signalling the singular nodal NFL present at the Mott quantum critical point.

To further probe the breakdown of coherent transport in the pseudogap (PG) regime, we examine the product

of the impurity spectral function $A(\omega)$ and the scattering lifetime $\tau(\omega)$, which approximates the optical conductivity $\sigma(\omega)$ via a Drude-type relation. As shown in the main panel of Fig. 9, this quantity exhibits a sharp Drude peak at $\omega = 0$ in the Fermi liquid (FL) regime (blue), consistent with long-lived quasiparticles. In stark contrast, the PG regime (green, red, orange) shows a pronounced suppression of low-frequency conductivity and the emergence of a finite-frequency peak centered near $\omega/D \sim 0.3-0.4$ (where D is the kinetic energy bandwidth).

Strikingly, this peak shifts very little across the PG regime (see inset), despite a deepening spectral gap and diverging self-energy. Its position lies well below the Mott gap ($\sim 2.5D$), suggesting that it represents an emergent mid-infrared (MIR) excitation intrinsic to the Mott metal characterising the PG. This feature closely mirrors the experimentally observed MIR peak in high-T_c cuprates [65–67], which has been variously attributed to excitations of electrons bound to vacancies [68], or the dressing of holes by spin excitations [69]. Here, its robust energy scale and insensitivity to increasing incoherence imply a universality persisting through the PG, likely rooted in short-range entanglement between deconfined doublons and holons excitations of the Mott metal. This is further evidence that the PG metal is not simply a degraded Fermi liquid, but a distinct phase whose optical response is driven by emergent degrees of freedom.

C. Non-local correlations in the pseudogap

In Fig. 10(a) and 10(b), the spin-flip correlations and mutual information between the impurity spin and conduction bath sites respectively are observed to undergo a crossover within the PG, from a short-ranged behaviour at its onset, to a long-ranged behaviour as the Mott transition approaches. The entanglement is also observed to be multipartite in nature: in Fig. 10(c), the quantum

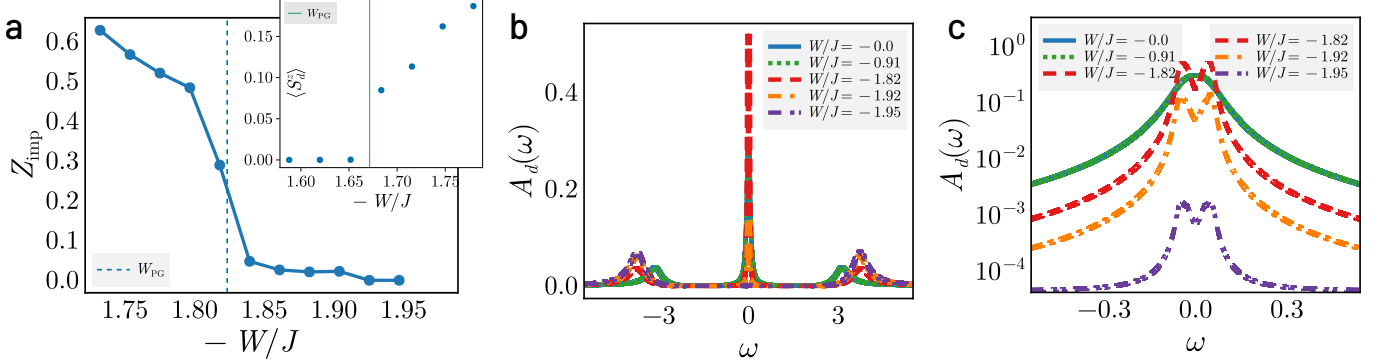


FIG. 6. (a) Suppression of quasiparticle residue (Z_{imp}) as the impurity model is tuned towards the Mott transition. An initial drastic fall in Z_{imp} is observed for $W/J \lesssim (W/J)_{\text{PG}}$ from 0.3 to around 0.05, signalling the destruction of the FL with unravelling of Kondo screening. A steady decrease in Z_{imp} is observed in passage through the PG, and is vanishingly small close to the Mott transition due to a divergent self-energy. Inset shows the growth of unscreened impurity magnetic moment in the pseudogap phase, signalling the breakdown of Kondo screening. (b) Impurity Spectral function in the FL and PG phases. The evolution of the central peak from Kondo resonance to pseudogap is accompanied by dynamical spectral weight transfer to the Hubbard side bands at finite frequencies $\omega \simeq \pm 3$ (in units of the bandwidth). (c) Zoom-in of the central (Kondo) resonance of the impurity spectral function. While undisturbed in the Fermi liquid phase, it splits into a pseudogap in the PG phase, with its height diminishing rapidly as the Mott transition is approached.

Fisher information (QFI) [70] computed for the ground state wavefunction using an operator corresponding to the sum of local spin-flip exchange processes shows a jump at the onset of the PG. Further, the FL is observed to possess bi-partite entanglement while the NFL of the PG phase displays pentapartite entanglement [71, 72].

These striking results imply that the Mott transition observed by us lies beyond the local quantum criticality scenario [73]. Instead, we observe the PG phase to be a novel state of strongly interacting quantum matter emergent from the breakdown of local Kondo screening. This state is described by a quantum critical Fermi surface [74] with NFL Fermi arcs that display increasingly critical behaviour, i.e., dynamics described by non-local quantum fluctuations, and excitations that become truly long-ranged close to the transition. It is tempting to conjecture that the long-range entangled critical state captured in Fig. 10(b) reflects the existence of a highly efficient scrambler [75–77], i.e., a state in which entanglement spreads among its constituents at the fastest rate permissible by quantum mechanics.

VI. EXACTLY SOLVABLE NODAL NON-FERMI LIQUID AT MOTTO CRITICALITY

Very close to the transition, the excitations of the nodal NFL correspond to those of a Hatsugai-Kohmoto model [47, 48]. This insight is obtained from a perturbation-theoretic treatment of the RG fixed point Hamiltonian of the impurity model for $W/J \lesssim (W/J)_{\text{PG}}$, by considering the effects of a small fixed point Kondo scattering probability J^* in the backdrop of a larger bath interaction parameter $|W|$. This yields the HK model [47, 48] as the singular part of the effective Hamil-

tonian arising from forward scattering processes (see Appendix B for details of the derivation).

The second-order renormalised Hamiltonian is

$$H_{\text{eff}} = \sum_{\mathbf{q}, \sigma} \epsilon_{\mathbf{q}} r_{\mathbf{q}, \sigma} + \mathcal{U} \sum_{\mathbf{q}, \sigma} r_{\mathbf{q}\sigma} r_{\mathbf{q}\bar{\sigma}} + \mathcal{U} \sum_{\mathbf{q}_1 \neq \mathbf{q}_2, \sigma} [r_{\mathbf{q}_1\sigma} r_{\mathbf{q}_2\bar{\sigma}} + \phi_{\mathbf{q}_1, \bar{\sigma}}^\dagger \phi_{\mathbf{q}_1, \sigma}^\dagger \phi_{\mathbf{q}_2, \sigma} \phi_{\mathbf{q}_2, \bar{\sigma}}^\dagger] . \quad (36)$$

where $\epsilon_{\mathbf{q}} = \text{sign}(\varepsilon_{\mathbf{N}_1 + \mathbf{q}}) \frac{\varepsilon_{\mathbf{N}_1 + \mathbf{q}}^2}{-W}$ and $\mathcal{U} = \frac{J^{*2}}{4W}$. The number operator $n_{\mathbf{q}\sigma} = \phi_{\mathbf{q}, \sigma}^\dagger \phi_{\mathbf{q}, \sigma}$ pertains to emergent fermionic relative modes $\phi_{\mathbf{q}, \sigma} = \frac{1}{\sqrt{2}} (c_{\mathbf{N}_1 + \mathbf{q}, \sigma} - c_{\mathbf{N}_1 + \mathbf{Q}_1 - \mathbf{q}, \sigma})$ that are shifted by an excitation momentum \mathbf{q} away from the nodal point $\mathbf{N}_1 = (\pi/2, \pi/2)$ and its partner $\mathbf{N}_1 + \mathbf{Q}_1 = (-\pi/2, -\pi/2)$. The $\mathbf{q}_1 = \mathbf{q}_2$ component of the Hamiltonian shows the emergence of the exactly solvable Hatsugai-Kohmoto model [47, 48] at the critical point. The correlation term $\mathcal{U} \sum_{\mathbf{q}, \sigma} r_{\mathbf{q}\sigma} r_{\mathbf{q}\bar{\sigma}}$ leads to a transfer of spectral weight across the Fermi surface and separates the available states into three classes:

$$\langle n_{\mathbf{q}} \rangle = \begin{cases} 2, & \epsilon_{\mathbf{q}} < -|\mathcal{U}/2| , \\ 1, & |\mathcal{U}/2| > \epsilon_{\mathbf{q}} > -|\mathcal{U}/2| , \\ 0, & |\mathcal{U}/2| < \epsilon_{\mathbf{q}} . \end{cases} \quad (37)$$

In contrast to a Fermi liquid, there is a highly degenerate single-occupied region in the middle, and this gives rise to non-Fermi liquid excitations.

We now discuss the effects of the $\mathbf{q}_1 \neq \mathbf{q}_2$ component. The first term partially lifts the degeneracy of the central singly-occupied region and allows only zero magnetisation configurations. The second term creates gapped excitations involving the regions of zero and double occupancy; these represent subdominant pairing fluctuations of the nodal non-Fermi liquid.

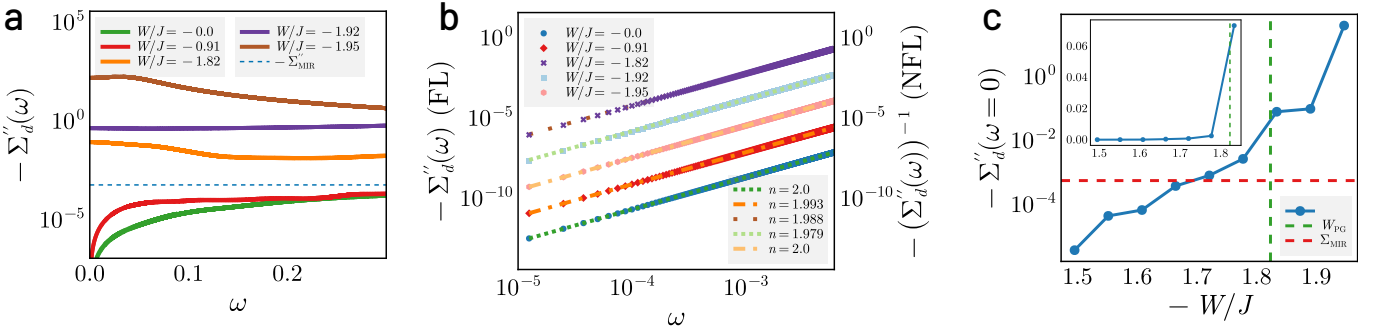


FIG. 7. (a) Imaginary part of impurity self-energy $\Sigma''(\omega)$ as a function of frequency ω for Fermi liquid (FL, $|W/J| < 1.79$) and pseudogapped phases (NFL, $|W/J| \geq 1.79$). $\Sigma''(\omega)$ falls to zero as $\omega \rightarrow 0$ for the FL, while it attains a peak in the pseudogap. All $\Sigma''(\omega)$ for the NFL are observed to lie above the Mott-Ioffe-Regel (MIR) bound (dashed blue line), while those for the FL lie below. (b) Scaling of $\Sigma''(\omega)$ with frequency for Fermi liquid and pseudogapped phases. The FL self-energy fits to $\Sigma'' \sim \omega^\alpha$ with $\alpha \approx 2$, vanishing as $\omega \rightarrow 0$, while the NFL self-energy grows as $\Sigma'' \approx a - \omega^\beta$ for small ω , with $\beta \approx 2$. Remarkably, the NFL exponent remains mostly unchanged through the entirety of the PG phase. (c) Variation of the zero-frequency imaginary self-energy $-\Sigma''(\omega = 0)$ with ω in the FL and pseudogap phases (entry into the PG is marked by the vertical dashed line). The inset shows the same but in linear scale, in order to display the dramatic rise (by almost 30 times) on entering the PG.

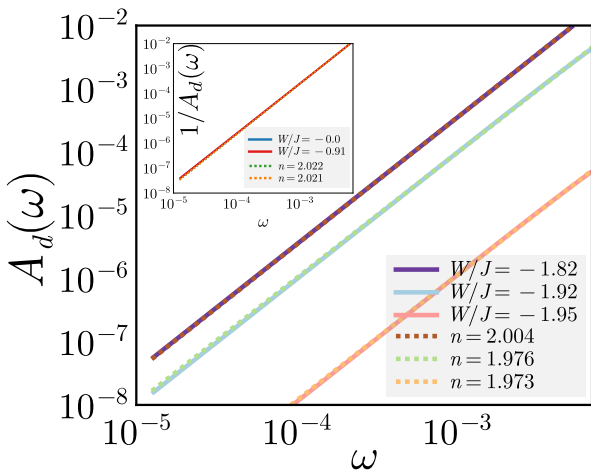


FIG. 8. Impurity spectral function $A_d(\omega)$ in the local Fermi liquid (inset) and pseudogap (main). The PG spectral function is fit to a power law (with the $\omega = 0$ contribution subtracted, see Fig. 7(c) for the full spectral function). The exponent of the power law comes out to be $n \approx 2$ throughout the PG. The local FL spectral function (inset) is fit to a lorentzian (by fitting the inverse to a power law).

Consequently, the resulting NFL metal of the lattice model involves long-lived excitations of multiple \mathbf{k} -states, and manifest in the form of a divergent one-particle self-energy at the non-interacting FS [78]: $\Sigma_{\mathbf{q}}(\omega) = -\mathcal{U}^2/4(\omega - \epsilon_{\mathbf{q}})$, such that $\Sigma_{\epsilon_{\mathbf{q}}=0}(\omega \rightarrow 0) \rightarrow \infty$. This zero-frequency self-energy pole presages the transition into a Mott insulating phase, where it marks a hard gap in the spectral function for charge excitations. This is consistent with our findings for the lattice (Fig. 5(c)) and impurity self-energies (Fig. 7(c)). The nodal Mott metal thus comprises of a Greens function zero at the Fermi energy together with an anisotropic massless Dirac dispersion, leading to a non-zero Chern number [79–81].

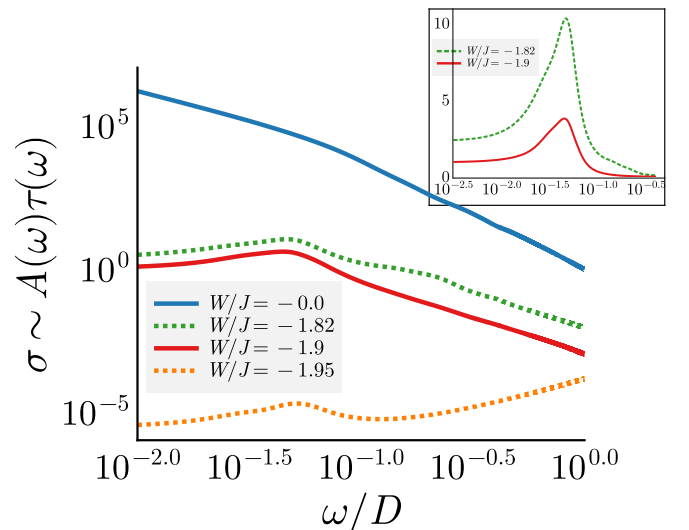


FIG. 9. Optical conductivity $\sigma(\omega)$ for excitations of the impurity model, approximated through the product of the carrier density (taken from the density of states $A(\omega)$) and the lifetime $\tau(\omega)$ (obtained from the inverse scattering rate $-1/\Sigma''(\omega)$, where Σ'' is the imaginary part of the self-energy). The Fermi liquid (blue) shows a sharp Drude peak at $\omega = 0$ due to the presence of long-lived quasiparticles. The PG (green, red, orange) shows a shifted Drude peak at a non-zero frequency which is reminiscent of the mid-infrared (MIR) peak seen experimentally in the cuprates [65–67]. Inset shows the robustness of the position of the MIR peak through the PG, indicating it as a universal feature of the Mott metal.

This topological index survives into the Mott insulator.

For small but non-zero values of $\omega - \epsilon_{\mathbf{k}}$, we obtain a quasiparticle residue that vanishes with ω , $Z_{\text{imp}} \sim \omega^2/\mathcal{U}^2$. The scattering rate of this singular NFL possesses a sharp peak at the FS ($\omega = \epsilon_{\mathbf{k}_F}$):

$$\Gamma \sim \mathcal{U}^2 \delta(\omega - \epsilon_{\mathbf{k}}), \quad (38)$$

consistent with the sharply peaked Lorentzian $\Sigma''_{\mathbf{k}}(\omega) \sim \omega^{-2}$ captured in Fig. 7(a). This quantum critical NFL metal is an example of a strongly coupled scale-invariant form of quantum matter. The exact solution for eq.(36) reveals the presence of low-energy excitations comprised of holons and doublons [47]. These features point to the nodal NFL as a long-ranged and multipartite entangled, strongly interacting scale-invariant state of quantum matter [2, 82–84] that are completely disconnected from the quasiparticles of the FL. Following the arguments laid out in [5], at finite temperatures, such a scale-invariant highly entangled non-Fermi liquid is likely associated with Planckian dissipation (i.e., $\Sigma''(T) \sim k_B T$) and a resistivity that varies linearly with temperature ($\rho \sim T$) [85–87]. This sits well with the possibility that this state is also a highly efficient scrambler [75–77]. Additionally, as mentioned above, we observe that the nodal metal possesses pairing fluctuations that can become dominant upon doping [78].

VII. PSEUDOGAP AS A STRONGLY COUPLED PHASE OF QUANTUM MATTER

We now unveil an organising principle that leads to the remarkable properties observed above for the strongly interacting NFL of the PG phase. The existence of a sharp connected FS at $T = 0$ can be understood as the existence of a topologically protected manifold of gapless chiral excitations in \mathbf{k} -space at the FS [50]. The FS is characterised by a topological index corresponding to an anomaly in the quantum many-body theory for electrons, and can be understood as a generalised symmetry of such a system [51, 88]. A theorem by Luttinger and Ward [89] shows that a count of the physical charge (known as Luttinger's volume) is identical to the topological index (a so-called homotopy charge known as Luttinger's count) even in the presence of electronic interactions that do not disturb the FS. We will now argue that the emergence of antinodal Luttinger surfaces involve a disconnection of the FS (into Fermi arcs) and that, by following La Nave et al. [51], the accompanying change in its topological properties leads to the existence of gapless NFL excitations that are non-local in nature.

The antinodal Luttinger surfaces arise from the splitting of double poles of the single-particle Greens function on the FS into poles lying on opposite complex half-planes, together with zeros that are pinned at the FS. These changes in the analytic structure of the single-particle Greens function have important consequences. First, the emergent zeros break a \mathbb{Z}_2 symmetry of the FS [41, 42, 51]. This symmetry is guaranteed within FL theory because the presence of quasiparticles vanishingly close to the FS allows the interchange of spin and charge degrees of freedom, promoting the separate $SU(2)$ symmetries of spin and charge to the larger symmetry of $O(4) = SU(2) \times SU(2) \times \mathbb{Z}_2$ [41]. The insertion of zeros of the Greens function at the Fermi surface in the

PG, and the associated splitting of the Greens function, breaks this \mathbb{Z}_2 symmetry by placing the pole for the spin excitation in one half of the complex plane while placing that for the charge excitation in the other half [42, 90].

Second, they signal a divergent electronic self-energy as a function of the wavevector \mathbf{k} , render ill-behaved the Luttinger-Ward functional of the interacting electronic problem, and violate the generalised symmetry encoded within it. The changes in the pole structure change the Luttinger count topological invariant, while the zeros give rise to an additional topological contribution (linked to the Adler-Bell-Jackiw-type chiral anomaly) [49, 81, 91, 92]. As a consequence of the half-filled particle-hole symmetric nature of the system at hand, Luttinger's volume is preserved upon taking into account topological contributions from both the Luttinger count *and* the zeros [40]. Importantly, La Nave et al. [51] argue, following recent developments in understanding generalised symmetries [93], that the additional anomaly arising from the Luttinger surfaces guarantees the existence of gapless NFL excitations that are non-local in nature.

Thus, the drastic change in nature of the real-space excitations - from locally well-defined Landau quasiparticles of the FL to the increasingly nonlocal excitations of the NFL Fermi arcs in the PG phase - appears to be dictated by a topological principle and, therefore, robust under renormalisation. This signals the NFL Fermi arcs of the PG as an emergent phase of strongly interacting quantum matter - which we dub the *Mott metal* - that is the parent metal of the MI. The same topological principle connects the nonlocal unparticle-like gapless excitations [2, 82–84] of the scale-invariant nodal NFL of the HK model observed precisely at the Mott critical point to those of the rest of the PG phase, e.g., a universal scaling of $\Sigma''_{\mathbf{k}}(\omega) \sim (a + \omega^2)^{-1}$ (Fig. 7(b)) and local density of states $A_d(\omega) \sim \omega^2$ (Fig. 8) of the NFL throughout the PG phase, such that the value of $\Sigma''_{\mathbf{k}}(\omega = 0)$ value continues to grow upon violating the MIR bound (Fig. 7(c)).

VIII. CONCLUSIONS

Our analysis reveals that the Mott transition proceeds via a continuous evolution through a PG regime characterized by a singular NFL metal - the Mott metal - with deconfined holon-doublon excitations confined to nodal Fermi arcs, and a scaling of its spectral features with universal power-law exponents. As the system approaches criticality, this metallic phase exhibits increasingly non-local correlations and a divergent self-energy, signalling the breakdown of Landau quasiparticles, formation of local moments and the onset of long-range quantum entanglement. Anchored in two-channel Kondo dynamics at intermediate scales and governed by Hatsugai-Kohmoto physics near the critical endpoint, the Mott metal provides a unified framework for understanding anomalous metallicity in strongly correlated systems. Its fate under

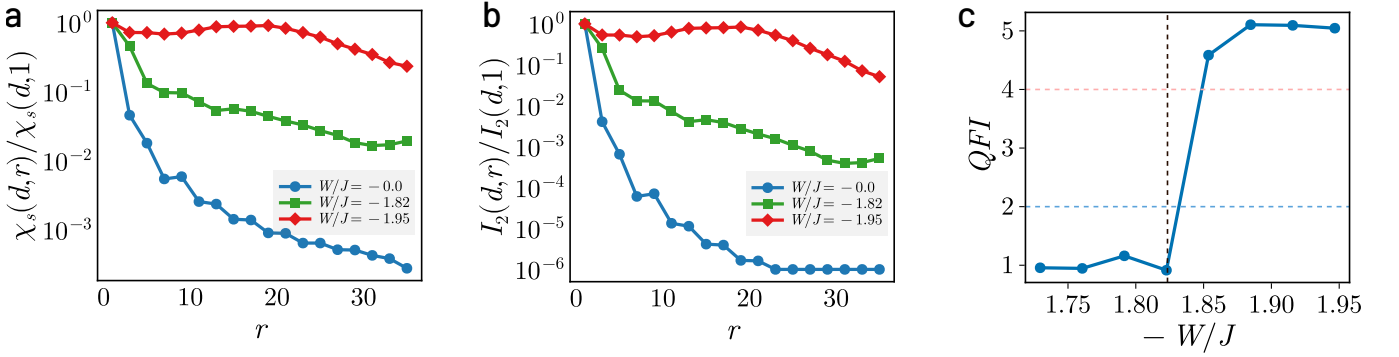


FIG. 10. (a) Spin correlation $\langle \mathbf{S}_d \cdot \mathbf{S}_r \rangle$ and (b) mutual information $I_2(d, r)$ between the impurity spin and conduction bath local spin density as a function of the distance r between them, normalised against the value at $r = 1$. Both decay very quickly in the FL phase (blue), but show long-ranged behaviour in the NFL phase (green and red), extending to the edges of the system at the critical point (red). (c) Evolution of the Quantum Fisher Information F_Q for a nearest-neighbour spin-flip operator $\mathcal{O} = \sum_{i \in \text{odd}} (S_i^+ S_{i+1}^- + \text{h.c.})$ through the first Lifshitz transition and the pseudogap. The vertical dashed line marks the onset of the PG. To the left of it, the QFI in the Fermi liquid phase shows at most bipartite entanglement ($F_Q < 2$ (below blue dashed line)), while the PG shows the presence of multipartite entanglement upto 5 parties ($F_Q > 4$ (red dashed line)).

finite doping presents a compelling direction for future investigation.

-
- [1] L. Landau, Soviet Physics Jete-Ussr **3**, 920 (1957).
- [2] P. W. Phillips, B. W. Langley, and J. A. Hutasoit, Phys. Rev. B **88**, 115129 (2013).
- [3] I. Dzyaloshinskii, Physical Review B **68**, 085113 (2003).
- [4] N. F. Mott, Proceedings of the Physical Society. Section A **62**, 416 (1949).
- [5] P. W. Phillips, N. E. Hussey, and P. Abbamonte, Science **377**, eabb4273 (2022).
- [6] A. G. Loeser, Z.-X. Shen, D. S. Dessau, D. S. Marshall, C. H. Park, P. Fournier, and A. Kapitulnik, Science **273**, 325 (1996).
- [7] M. R. Norman, H. Ding, M. Randeria, J. C. Campuzano, T. Yokoya, T. Takeuchi, T. Takahashi, T. Mochiku, K. Kadokawa, P. Guptasarma, and D. G. Hinks, Nature **392**, 157 (1998).
- [8] M. Hashimoto, I. M. Vishik, R.-H. He, T. P. Devereaux, and Z.-X. Shen, Nature Physics **10**, 483 (2014).
- [9] L. Taillefer, Annual Review of Condensed Matter Physics **1**, 51 (2010).
- [10] E. Fradkin, S. A. Kivelson, and J. M. Tranquada, Rev. Mod. Phys. **87**, 457 (2015).
- [11] Y. Sato, S. Kasahara, H. Murayama, Y. Kasahara, E.-G. Moon, T. Nishizaki, T. Loew, J. Porras, B. Keimer, T. Shibauchi, and Y. Matsuda, Nature Physics **13**, 1074 (2017).
- [12] N. Doiron-Leyraud, O. Cyr-Choinière, S. Badoux, A. Ataei, C. Collignon, A. Gourgout, S. Dufour-Beauséjour, F. F. Tafti, F. Laliberté, M.-E. Boulanger, M. Matusiak, D. Graf, M. Kim, J.-S. Zhou, N. Momono, T. Kurosawa, H. Takagi, and L. Taillefer, Nature Communications **8**, 2044 (2017).
- [13] S. Mukhopadhyay, R. Sharma, C. K. Kim, S. D. Edkins, M. H. Hamidian, H. Eisaki, S. ichi Uchida, E.-A. Kim, M. J. Lawler, A. P. Mackenzie, J. C. S. Davis, and K. Fujita, Proceedings of the National Academy of Sciences **116**, 13249 (2019).
- [14] N. K. Gupta, C. McMahon, R. Sutarto, T. Shi, R. Gong, H. I. Wei, K. M. Shen, F. He, Q. Ma, M. Dragomir, B. D. Gaulin, and D. G. Hawthorn, Proceedings of the National Academy of Sciences **118**, e2106881118 (2021).
- [15] M. Horio, S. Sakai, H. Suzuki, Y. Nonaka, M. Hashimoto, D. Lu, Z.-X. Shen, T. Ohgi, T. Konno, T. Adachi, Y. Koike, M. Imada, and A. Fujimori, Proceedings of the National Academy of Sciences **122**, e2406624122 (2025).
- [16] B. Kyung, S. S. Kancharla, D. Sénéchal, A.-M. S. Tremblay, M. Civelli, and G. Kotliar, Phys. Rev. B **73**, 165114 (2006).
- [17] A. Macridin, M. Jarrell, T. Maier, P. R. C. Kent, and E. D'Azevedo, Phys. Rev. Lett. **97**, 036401 (2006).
- [18] S. Sakai, Y. Motome, and M. Imada, Physical review letters **102**, 056404 (2009).
- [19] P. Werner, E. Gull, O. Parcollet, and A. J. Millis, Physical Review B **80**, 045120 (2009).
- [20] S. Sakai, Y. Motome, and M. Imada, Physical Review B **82**, 134505 (2010).
- [21] N. Lin, E. Gull, and A. J. Millis, Phys. Rev. B **82**, 045104 (2010).
- [22] E. Gull, M. Ferrero, O. Parcollet, A. Georges, and A. J. Millis, Physical Review B **82**, 155101 (2010).
- [23] E. Gull and A. J. Millis, Phys. Rev. B **86**, 241106 (2012).
- [24] S. I. Mirzaei, D. Stricker, J. N. Hancock, C. Berthod, A. Georges, E. van Heumen, M. K. Chan, X. Zhao, Y. Li, M. Greven, N. Barišić, and D. van der Marel, Proceedings of the National Academy of Sciences **110**, 5774 (2013).
- [25] E. Gull, O. Parcollet, and A. J. Millis, Physical review letters **110**, 216405 (2013).
- [26] A. Mukherjee and S. Lal, New Journal of Physics **22**, 063008 (2020).
- [27] C. Hille, D. Rohe, C. Honerkamp, and S. Andergassen, Phys. Rev. Res. **2**, 033068 (2020).
- [28] W. Jiang, Y. Liu, A. Klein, Y. Wang, K. Sun, A. V. Chubukov, and Z. Y. Meng, Nature Communications **13**,

- 2655 (2022).
- [29] M. S. Scheurer, S. Chatterjee, W. Wu, M. Ferrero, A. Georges, and S. Sachdev, *Proceedings of the National Academy of Sciences* **115**, E3665 (2018).
- [30] F. Krien, P. Worm, P. Chalupa-Gantner, A. Toschi, and K. Held, *Communications Physics* **5**, 336 (2022).
- [31] M. Kitatani, L. Si, P. Worm, J. M. Tomczak, R. Arita, and K. Held, *Phys. Rev. Lett.* **130**, 166002 (2023).
- [32] S. Sorella, *Phys. Rev. B* **107**, 115133 (2023).
- [33] T. Schäfer, N. Wentzell, F. Šimkovic, Y.-Y. He, C. Hille, M. Klett, C. J. Eckhardt, B. Arzhang, V. Harkov, F. m. c.-M. Le Régent, A. Kirsch, Y. Wang, A. J. Kim, E. Kozik, E. A. Stepanov, A. Kauch, S. Andergassen, P. Hansmann, D. Rohe, Y. M. Vilk, J. P. F. LeBlanc, S. Zhang, A.-M. S. Tremblay, M. Ferrero, O. Parcollet, and A. Georges, *Phys. Rev. X* **11**, 011058 (2021).
- [34] S. R. White and D. J. Scalapino, *Phys. Rev. Lett.* **80**, 1272 (1998).
- [35] K. Ido, T. Ohgoe, and M. Imada, *Phys. Rev. B* **97**, 045138 (2018).
- [36] C. Proust and L. Taillefer, *Annual Review of Condensed Matter Physics* **10**, 409 (2019).
- [37] B. Ponsioen, S. S. Chung, and P. Corboz, *Phys. Rev. B* **100**, 195141 (2019).
- [38] H. Xu, H. Shi, E. Vitali, M. Qin, and S. Zhang, *Phys. Rev. Res.* **4**, 013239 (2022).
- [39] K. B. Dave, P. W. Phillips, and C. L. Kane, *Phys. Rev. Lett.* **110**, 090403 (2013).
- [40] K. Seki and S. Yunoki, *Physical Review B* **96**, 085124 (2017).
- [41] P. W. Anderson and F. D. M. Haldane, *Journal of Statistical Physics* **103**, 425 (2001).
- [42] E. W. Huang, G. L. Nave, and P. W. Phillips, *Nature Physics* **18**, 511 (2022).
- [43] P. Coleman, C. Pépin, Q. Si, and R. Ramazashvili, *Journal of Physics: Condensed Matter* **13**, R723 (2001).
- [44] A. Mukherjee and S. Lal, *Nuclear Physics B* **960**, 115170 (2020).
- [45] A. Mukherjee and S. Lal, *Nuclear Physics B* **960**, 115163 (2020).
- [46] B. Keimer, S. A. Kivelson, M. R. Norman, S. Uchida, and J. Zaanen, *Nature* **518**, 179 (2015).
- [47] Y. Hatsugai and M. Kohmoto, *Journal of the Physical Society of Japan* **61**, 2056 (1992).
- [48] G. Baskaran, *Modern Physics Letters B* **05**, 643 (1991).
- [49] B. L. Altshuler, A. V. Chubukov, A. Dashevskii, A. M. Finkel'stein, and D. K. Morr, *Europhysics Letters* **41**, 401 (1998).
- [50] J. T. Heath and K. S. Bedell, *New Journal of Physics* **22**, 063011 (2020).
- [51] G. L. Nave, J. Zhao, and P. W. Phillips, (2025), arXiv:2506.04342 [cond-mat.str-el].
- [52] S. Pal, A. Mukherjee, and S. Lal, *New Journal of Physics* **21**, 023019 (2019).
- [53] A. Mukherjee, S. Patra, and S. Lal, *Journal of High Energy Physics* **2021**, 148 (2021).
- [54] A. Mukherjee and S. Lal, *New Journal of Physics* **22**, 063007 (2020).
- [55] S. Patra and S. Lal, *Phys. Rev. B* **104**, 144514 (2021).
- [56] A. Mukherjee, A. Mukherjee, N. S. Vidhyadhiraja, A. Taraphder, and S. Lal, *Phys. Rev. B* **105**, 085119 (2022).
- [57] S. Patra, A. Mukherjee, and S. Lal, *New Journal of Physics* **25**, 063002 (2023).
- [58] A. Stoyanova, *Delocalized and correlated wave functions for excited states in extended systems*, Ph.D. thesis, University of Groningen (2006).
- [59] A. Mukherjee, N. S. Vidhyadhiraja, A. Taraphder, and S. Lal, *New Journal of Physics* **25**, 113011 (2023).
- [60] W. Wu, M. S. Scheurer, S. Chatterjee, S. Sachdev, A. Georges, and M. Ferrero, *Phys. Rev. X* **8**, 021048 (2018).
- [61] A. M. Tsvelick and P. B. Wiegmann, *Journal of Statistical Physics* **38**, 125 (1985).
- [62] V. J. Emery and S. Kivelson, *Phys. Rev. B* **46**, 10812 (1992).
- [63] O. Gunnarsson, M. Calandra, and J. E. Han, *Rev. Mod. Phys.* **75**, 1085 (2003).
- [64] N. E. Hussey, K. Takenaka, and H. Takagi, *Philosophical Magazine* **84**, 2847 (2004).
- [65] S. L. Herr, K. Kamarás, C. D. Porter, M. G. Doss, D. B. Tanner, D. A. Bonn, J. E. Greedan, C. V. Stager, and T. Timusk, *Phys. Rev. B* **36**, 733 (1987).
- [66] J. Orenstein, G. A. Thomas, D. H. Rapkine, C. G. Bethea, B. F. Levine, R. J. Cava, E. A. Rietman, and D. W. Johnson, *Phys. Rev. B* **36**, 729 (1987).
- [67] S. Uchida, T. Ido, H. Takagi, T. Arima, Y. Tokura, and S. Tajima, *Phys. Rev. B* **43**, 7942 (1991).
- [68] G. A. Thomas, D. H. Rapkine, S. L. Cooper, S.-W. Cheong, A. S. Cooper, L. F. Schneemeyer, and J. V. Waszczak, *Phys. Rev. B* **45**, 2474 (1992).
- [69] E. Dagotto, *Rev. Mod. Phys.* **66**, 763 (1994).
- [70] P. Hauke, M. Heyl, L. Tagliacozzo, and P. Zoller, *Nature Physics* **12**, 778 (2016).
- [71] D. Balut, X. Guo, N. de Vriesa, D. Chaudhuri, B. Bradlyn, P. Abbamonte, and P. P. W., *Physica C* **635**, 1354750 (2025).
- [72] F. Mazza, S. Biswas, X. Yan, A. Prokofiev, P. Steffens, Q. Si, F. F. Assaad, and S. Paschen, (2024), arXiv:2403.12779 [cond-mat.str-el].
- [73] Q. Si, S. Rabello, K. Ingersent, and J. L. Smith, *Nature* **413**, 804 (2001).
- [74] T. Senthil, *Phys. Rev. B* **78**, 035103 (2008).
- [75] Y. Sekino and L. Susskind, *Journal of High Energy Physics* **2008**, 065 (2008).
- [76] P. Hayden and J. Preskill, *Journal of High Energy Physics* **2007**, 120 (2007).
- [77] G. Bentsen, T. Hashizume, A. S. Buyskikh, E. J. Davis, A. J. Daley, S. S. Gubser, and M. Schleier-Smith, *Phys. Rev. Lett.* **123**, 130601 (2019).
- [78] P. W. Phillips, L. Yeo, and E. W. Huang, *Nature Physics* **16**, 1175 (2020).
- [79] O. Vafek and A. Vishwanath, *Annual Review of Condensed Matter Physics* **5**, 83 (2014).
- [80] T. Morimoto and N. Nagaosa, *Sci. Rep.* **6**, 19853 (2016).
- [81] R. Flores-Calderón and C. Hooley, *Phys. Rev. B* **111**, 235139 (2025).
- [82] H. Georgi, *Phys. Rev. Lett.* **98**, 221601 (2007).
- [83] H. Georgi, *Physics Letters B* **650**, 275 (2007).
- [84] P. W. Phillips, in *Quantum Criticality in Condensed Matter*, edited by J. Jedrzejewski (World Scientific, Singapore, 2014) pp. 133–158.
- [85] J. Zaanen, *SciPost Phys.* **6**, 061 (2019).
- [86] A. Legros, S. Benhabib, W. Tabis, F. Laliberté, M. Dion, M. Lizaire, B. Vignolle, D. Vignolles, H. Raffy, Z. Li, *et al.*, *Nature Physics* **15**, 142 (2019).
- [87] S. A. Hartnoll and A. P. Mackenzie, *Rev. Mod. Phys.* **94**, 041002 (2022).

- [88] J. McGreevy, Annual Review of Condensed Matter Physics **14**, 57 (2023).
- [89] J. M. Luttinger and J. C. Ward, Physical Review **118**, 1417 (1960).
- [90] L. Su and I. Martin, (2025), arXiv:2405.08093 [cond-mat.str-el].
- [91] S. L. Adler, Physical Review **177**, 2426 (1969).
- [92] J. S. Bell and R. Jackiw, Il Nuovo Cimento A **60**, 47 (1969).
- [93] H. Casini and J. M. Magán, Modern Physics Letters A **36**, 2130025 (2021).

ACKNOWLEDGMENTS

We acknowledge National Supercomputing Mission (NSM) for providing computing resources of ‘PARAM RUDRA’ at Aruna Asaf Ali Marg, near Vasant Kunj, Vasant Kunj, New Delhi, Delhi 110067, which is implemented by C-DAC and supported by the Ministry of Electronics and Information Technology (MeitY) and Department of Science and Technology (DST), Government of India. SL thanks the SERB, Govt. of India for funding through MATRICS grant MTR/2021/000141 and Core Research Grant CRG/2021/000852. AM thanks IISER Kolkata for funding through a JRF and an SRF. A.M. would also like to acknowledge the SERB-MATRICS grant (Grant No. MTR/2022/000636) from the Science and Engineering Research Board (SERB) for funding. S.L. thanks Mayank Shreshtha for designing Fig.1, and Deepshikha Jaiswal-Nagar for comments on the manuscript.

IX. CODE AND DATA AVAILABILITY

The codes created during this research are available from the corresponding author upon reasonable request.

Appendix A: Derivation of unitary RG equations for the lattice-embedded impurity model

Following Refs. [44, 54], at any given step j of the RG procedure, we decouple the states $\{\mathbf{q}\}$ on the isoenergetic surface of energy ε_j . The diagonal Hamiltonian H_D for this step consists of all terms that do not change the occupancy of the states $\{\mathbf{q}\}$:

$$H_D^{(j)} = \varepsilon_j \sum_{q,\sigma} \tau_{q,\sigma} + \frac{1}{2} \sum_{\mathbf{q}} J_{\mathbf{q},\mathbf{q}} S_d^z (\hat{n}_{\mathbf{q},\uparrow} - \hat{n}_{\mathbf{q},\downarrow}) - \frac{1}{2} \sum_{\mathbf{q}} W_{\mathbf{q}} (\hat{n}_{\mathbf{q},\uparrow} - \hat{n}_{\mathbf{q},\downarrow})^2 , \quad (\text{A1})$$

where $\tau = \hat{n} - 1/2$ and $W_{\mathbf{q}}$ is a shorthand for $W_{\mathbf{q},\mathbf{q},\mathbf{q},\mathbf{q}}$. The three terms, respectively, are the kinetic energy of the momentum states on the isoenergetic shell that we are decoupling, the spin-correlation energy between the impurity spin and the spins formed by these momentum states and, finally, the local correlation energy associated with these states arising from the W term. The off-diagonal part of the Hamiltonian on the other hand leads to scattering in the states $\{\mathbf{q}\}$.

The renormalisation of the Hamiltonian is constructed from the general expression [44, 54]

$$\Delta H^{(j)} = H_X \frac{1}{\omega - H_D} H_X . \quad (\text{A2})$$

1. Renormalisation of the bath correlation term W

The bath correlation term W can undergo renormalisation only via scattering processes arising from itself. Irrespective of whether the state \mathbf{q} being decoupled is in a particle or hole configuration in the initial many-body state, the propagator $G = 1/(\omega - H_D)$ of the intermediate excited state is uniform, and equal to

$$G_W = 1/(\omega - |\varepsilon_j|/2 + W_{\mathbf{q}}/2) , \quad (\text{A3})$$

where $W_{\mathbf{q}}$ is the same whether \mathbf{q} is above or below the Fermi surface. The $|\varepsilon_j|/2$ in H_D arises from the excited nature of the state after the initial scattering process.

a. Scattering arising purely from spin-preserving processes

One possible set of processes gives

$$T_{P1}^\dagger G_W T_{P3} = - \sum_{\sigma} \sum_{\mathbf{k}_1, \mathbf{k}_2, \mathbf{k}_3, \mathbf{k}_4} c_{\mathbf{k}_1, \sigma}^\dagger c_{\mathbf{k}_2, \sigma} c_{\mathbf{k}_3, \sigma}^\dagger c_{\mathbf{k}_4, \sigma} \sum_{\mathbf{q} \in \text{PS}} W_{\mathbf{q}, \mathbf{k}_2, \mathbf{k}_3, \mathbf{k}_4} G_W W_{\mathbf{k}_1, \mathbf{q}, \mathbf{q}, \mathbf{q}} . \quad (\text{A4})$$

The second such contribution is obtained by flipping the sequence of scattering processes:

$$T_{P3} G_W T_{P1}^\dagger = \sum_{\sigma} \sum_{\mathbf{k}_1, \mathbf{k}_2, \mathbf{k}_3, \mathbf{k}_4} c_{\mathbf{k}_1, \sigma}^\dagger c_{\mathbf{k}_2, \sigma} c_{\mathbf{k}_3, \sigma}^\dagger c_{\mathbf{k}_4, \sigma} \sum_{\mathbf{q} \in \text{HS}} W_{\mathbf{q}, \mathbf{k}_2, \mathbf{k}_3, \mathbf{k}_4} G_W W_{\mathbf{k}_1, \mathbf{q}, \mathbf{q}, \mathbf{q}} . \quad (\text{A5})$$

The product of couplings $W_{\mathbf{q}, \mathbf{k}_2, \mathbf{k}_3, \mathbf{k}_4} G_W W_{\mathbf{k}_1, \mathbf{q}, \mathbf{q}, \mathbf{q}}$ is the same irrespective of whether \mathbf{q} belongs to the particle or hole sector. The two contributions therefore cancel each other.

b. Scattering arising from spin-flip processes

We now come to the processes that involve spin-flips. The first class of processes is

$$\begin{aligned} T_{F1}^\dagger G_W T_{F4} &= - \sum_{1,2,3,4} \sum_{\sigma} c_{\mathbf{k}_1 \sigma}^\dagger c_{\mathbf{k}_2 \sigma} c_{\mathbf{k}_3 \bar{\sigma}}^\dagger c_{\mathbf{k}_4 \bar{\sigma}} \sum_{\mathbf{q} \in \text{PS}} W_{\mathbf{q}, \mathbf{k}_2, \mathbf{k}_4, \mathbf{k}_4} G_W W_{\mathbf{k}_1, \mathbf{q}, \mathbf{q}, \mathbf{q}} , \\ T_{F4} G_W T_{F1}^\dagger &= \sum_{1,2,3,4} \sum_{\sigma} c_{\mathbf{k}_1 \sigma}^\dagger c_{\mathbf{k}_2 \sigma} c_{\mathbf{k}_3 \bar{\sigma}}^\dagger c_{\mathbf{k}_4 \bar{\sigma}} \sum_{\mathbf{q} \in \text{HS}} W_{\mathbf{q}, \mathbf{k}_2, \mathbf{k}_4, \mathbf{k}_4} G_W W_{\mathbf{k}_1, \mathbf{q}, \mathbf{q}, \mathbf{q}} . \end{aligned} \quad (\text{A6})$$

By the same arguments as in the previous subsection, these terms cancel each other out.

The other two terms also cancel out for the same reason:

$$\begin{aligned} T_{F2}G_WT_{F2} &= \sum_{1,2,3,4} \sum_{\sigma} c_{\mathbf{k}_1\sigma}^{\dagger} c_{\mathbf{k}_2\sigma} c_{\mathbf{k}_3\bar{\sigma}}^{\dagger} c_{\mathbf{k}_4\bar{\sigma}} \sum_{\mathbf{q} \in PS} W_{\mathbf{q},\bar{\mathbf{q}},\mathbf{k}_3,\mathbf{k}_4} G_W W_{\bar{\mathbf{q}},\mathbf{q},\mathbf{k}_1,\mathbf{k}_2} , \\ T_{F3}G_WT_{F3} &= - \sum_{1,2,3,4} \sum_{\sigma} c_{\mathbf{k}_1\sigma}^{\dagger} c_{\mathbf{k}_2\sigma} c_{\mathbf{k}_3\bar{\sigma}}^{\dagger} c_{\mathbf{k}_4\bar{\sigma}} \sum_{\mathbf{q} \in PS} W_{\mathbf{q},\mathbf{k}_2,\mathbf{k}_3,\bar{\mathbf{q}}} G_W W_{\bar{\mathbf{q}},\mathbf{k}_4,\mathbf{k}_1,\mathbf{q}} , \end{aligned} \quad (A7)$$

c. Scattering involving both spin-flip and spin-preserving processes

These processes involve the combination of terms like T_{P1} with T_{F4} , and T_{P2} with T_{F1} . These again cancel each other out for the same reasons as outline above.

d. Net renormalisation for the bath correlation term

Since all the contributions cancel out in pairs, the bath correlation term W is *marginal*.

2. Renormalisation of the Kondo scattering term J

We focus on the renormalisation of the spin-flip part of the Kondo interaction. For these processes, the intermediate many-body state always involves the impurity spin being anti-correlated with the conduction electron spin, such that the propagator for that state is $G_J = 1/(\omega - |\varepsilon_j|/2 + J_{\mathbf{q}}/4 + W_{\mathbf{q}}/2)$.

a. Impurity-mediated spin-flip scattering purely through Kondo-like processes

The following processes arising from the Kondo term renormalise the spin-flip interaction:

$$T_{KT1}^{\dagger}G_J(T_{KZ1} + T_{KZ1}^{\dagger}) = -\frac{1}{8} \sum_{\mathbf{k}_1, \mathbf{k}_1} S_d^+ c_{\mathbf{k}_1\downarrow}^{\dagger} c_{\mathbf{k}_2\uparrow} \sum_{\mathbf{q} \in PS} [J_{\mathbf{q},\mathbf{k}_2} J_{\mathbf{k}_1,\mathbf{q}} + J_{\bar{\mathbf{q}},\mathbf{k}_1} J_{\mathbf{k}_2,\bar{\mathbf{q}}}] G_J . \quad (A8)$$

An identical contribution is obtained by switching the sequence of processes:

$$(T_{KZ1} + T_{KZ1}^{\dagger}) G_J T_{KT1}^{\dagger} = -\frac{1}{8} \sum_{\mathbf{k}_1, \mathbf{k}_1} S_d^+ c_{\mathbf{k}_1\downarrow}^{\dagger} c_{\mathbf{k}_2\uparrow} \sum_{\mathbf{q} \in PS} [J_{\bar{\mathbf{q}},\mathbf{k}_2} J_{\mathbf{k}_1,\bar{\mathbf{q}}} + J_{\mathbf{q},\mathbf{k}_1} J_{\mathbf{k}_2,\mathbf{q}}] G_J . \quad (A9)$$

b. Scattering processes involving interplay between the Kondo interaction and conduction bath interaction

$$T_{KT1}^{\dagger}G_J(T_{F4} + T_{F4}^{\dagger}) = \frac{1}{2} \sum_{\mathbf{k}_1, \mathbf{k}_2, \mathbf{q}} J_{\mathbf{k}_2, \mathbf{q}} S_d^+ \left(c_{\mathbf{q}\downarrow}^{\dagger} c_{\mathbf{k}_2\uparrow} G_J W_{\mathbf{q},\mathbf{q},\mathbf{k}_1,\mathbf{q}} n_{q\uparrow} c_{\mathbf{k}_1\downarrow}^{\dagger} c_{\mathbf{q}\downarrow} + c_{\mathbf{k}_2\downarrow}^{\dagger} c_{\mathbf{q}\uparrow} G_J W_{\bar{\mathbf{q}},\bar{\mathbf{q}},\mathbf{k}_1} n_{\bar{q}\downarrow} c_{\mathbf{q}\uparrow}^{\dagger} c_{\mathbf{k}_1\uparrow} \right) . \quad (A10)$$

For either of the two choices of the functional form of W , it is easy to show that $W_{\mathbf{q},\mathbf{q},\mathbf{k}_1,\mathbf{q}} = W_{\bar{\mathbf{q}},\bar{\mathbf{q}},\mathbf{k}_1}$.

$$T_{KT1}^{\dagger}G_J(T_{F4} + T_{F4}^{\dagger}) = \frac{1}{2} \sum_{\mathbf{k}_1, \mathbf{k}_2, \mathbf{q}} J_{\mathbf{k}_2, \mathbf{q}} W_{\mathbf{q},\mathbf{q},\mathbf{k}_1,\mathbf{q}} G_J S_d^+ \left[-c_{\mathbf{k}_1\downarrow}^{\dagger} c_{\mathbf{k}_2\uparrow} n_{\mathbf{q}\downarrow} n_{q\uparrow} + c_{\mathbf{k}_2\downarrow}^{\dagger} c_{\mathbf{k}_1\uparrow} (1 - n_{\mathbf{q}\uparrow}) n_{\bar{q}\downarrow} \right] . \quad (A11)$$

Another contribution is obtained by switching the sequence of the scattering processes:

$$(T_{F4} + T_{F4}^{\dagger}) G_J T_{KT1}^{\dagger} = \frac{1}{2} \sum_{\mathbf{k}_1, \mathbf{k}_2, \mathbf{q}} \left(c_{\mathbf{k}_1\downarrow}^{\dagger} c_{\mathbf{k}_2\uparrow} n_{\bar{q}\uparrow} (1 - n_{\mathbf{q}\downarrow}) - c_{\mathbf{k}_2\downarrow}^{\dagger} c_{\mathbf{k}_1\uparrow} n_{q\downarrow} n_{\mathbf{q}\uparrow} \right) W_{\mathbf{q},\mathbf{q},\mathbf{k}_1,\mathbf{q}} G_J J_{\mathbf{k}_2,\mathbf{q}} S_d^+ \quad (A12)$$

The two contributions (eqs. A11 and A12) arising from T_{KT1} cancel each other.

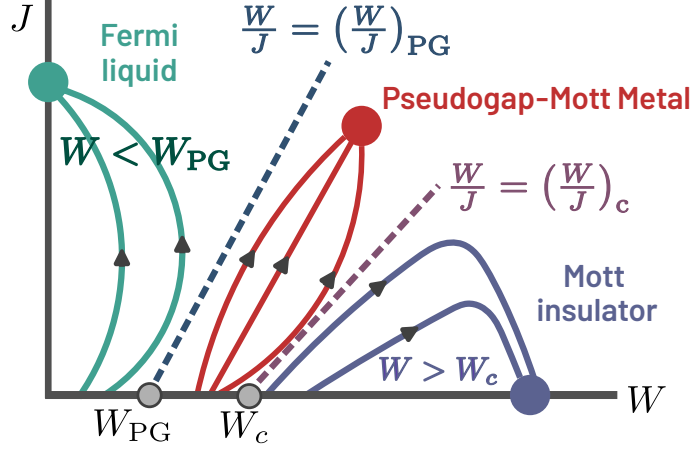


FIG. 11. Renormalisation group (RG) flow diagram of the lattice model as obtained from a unitary RG analysis of the lattice-embedded impurity model. For $|W/J| < |W/J|_{PG}$, the flows lead to a Fermi liquid phase, while for $|W/J| < |W/J|_c$, they lead to a Mott insulator. For values in between, the system flows to a Mott metal phase that has a pseudogap in the density of states.

We now consider the other spin-exchange process T_{KT2}^\dagger . One such contribution is

$$T_{KT2}^\dagger G_J T_{F3} = -\frac{1}{2} \sum_{\mathbf{k}_1, \mathbf{k}_2} S_d^+ c_{\mathbf{k}_1 \downarrow}^\dagger c_{\mathbf{k}_2 \uparrow} \sum_{\mathbf{q} \in PS} (J_{\mathbf{q}, \bar{\mathbf{q}}} W_{\bar{\mathbf{q}}, \mathbf{k}_2, \mathbf{k}_1, \mathbf{q}} + J_{\bar{\mathbf{q}}, \mathbf{q}} W_{\mathbf{q}, \mathbf{k}_2, \mathbf{k}_1, \bar{\mathbf{q}}}) G_J . \quad (A13)$$

An identical contribution is obtained from the reversed term:

$$T_{F3} G_J T_{KT2}^\dagger = -\frac{1}{2} \sum_{\mathbf{k}_1, \mathbf{k}_2} S_d^+ c_{\mathbf{k}_1 \downarrow}^\dagger c_{\mathbf{k}_2 \uparrow} \sum_{\mathbf{q} \in PS} (J_{\mathbf{q}, \bar{\mathbf{q}}} W_{\bar{\mathbf{q}}, \mathbf{k}_2, \mathbf{k}_1, \mathbf{q}} + J_{\bar{\mathbf{q}}, \mathbf{q}} W_{\mathbf{q}, \mathbf{k}_2, \mathbf{k}_1, \bar{\mathbf{q}}}) G_J . \quad (A14)$$

c. Net renormalisation to the Kondo interaction

Combining the results, the total renormalisation in the momentum-resolved Kondo coupling $J^{(j)}$ at the j^{th} step amounts to

$$\Delta J_{\mathbf{k}_1, \mathbf{k}_2}^{(j)} = - \sum_{\mathbf{q} \in PS} \frac{J_{\mathbf{k}_2, \mathbf{q}}^{(j)} J_{\mathbf{q}, \mathbf{k}_1}^{(j)} + 4 J_{\mathbf{q}, \bar{\mathbf{q}}}^{(j)} W_{\bar{\mathbf{q}}, \mathbf{k}_2, \mathbf{k}_1, \mathbf{q}}}{\omega - \frac{1}{2} |\varepsilon_j| + J_{\mathbf{q}}^{(j)} / 4 + W_{\mathbf{q}} / 2} \quad (A15)$$

A representation of the RG phase diagram in the $-W/t$ vs. J/t plane of couplings has been provided in Fig.2(a) from detailed numerical computations of eq.(A15). We also provide a schematic representation of RG flows to various fixed point theories in the J vs. W plane of couplings in Fig.11. This schematic figure shows the existence of three distinct phases (Fermi liquid metal, Mott Insulator, and Pseudogap-Mott metal) described by distinct fixed point theories of the RG flows. The Fermi liquid metal and Mott Insulator phases are distinguished from the Pseudogap-Mott metal by separatrices of the RG flows.

Appendix B: Theory for the nodal non-Fermi liquid as an effective Hatsugai-Kohmoto model

As the bath interaction W is tuned through the L-PG phase, the nodal region is the last to decouple from the impurity. This allows us to write down a simpler Kondo model near the transition, where only the nodal region is hybridising with the impurity spin through Kondo interactions. This is done by retaining only those scattering processes $\mathbf{k}_1 \rightarrow \mathbf{k}_2$ that originate from and end at k -points within a small neighborhood of width $|\mathbf{q}|$ around the four nodal points: $\mathbf{k}_1, \mathbf{k}_2 \in \mathbf{N} + \mathbf{q}$, $|\mathbf{q}| \ll \pi$, where \mathbf{N} can be any one of the four nodal points $\mathbf{N}_1 = (\pi/2, \pi/2)$, $\mathbf{N}_2 = (-\pi/2, \pi/2)$ and $\mathbf{N}_1 + \mathbf{Q}_1$ and $\mathbf{N}_2 + \mathbf{Q}_2$, where $\mathbf{Q}_1 = (-\pi, -\pi)$ and $\mathbf{Q}_2 = (\pi, -\pi)$ are the two nesting vectors. We assume that the window of \mathbf{q} is small enough so that the fixed point Kondo coupling values $J^*(\mathbf{q}_1, \mathbf{q}_2)$ for the scattering processes involving \mathbf{q}_1 and \mathbf{q}_2 can be replaced by an average value J^* .

With these considerations, the simplified low-energy model near the transition describing the Kondo scattering processes can be written as

$$\tilde{H}_{\text{imp-cbath}} = J^* \frac{1}{2} \sum_{l=1,2} \sum_{\mathbf{q}_1, \mathbf{q}_2} \sum_{\alpha, \beta} \mathbf{S}_d \cdot \boldsymbol{\sigma}_{\alpha\beta} \left(c_{\mathbf{N}_l + \mathbf{q}_1, \alpha}^\dagger c_{\mathbf{N}_l + \mathbf{q}_2, \beta} + c_{\mathbf{N}_l + \mathbf{Q}_l + \mathbf{q}_1, \alpha}^\dagger c_{\mathbf{N}_l + \mathbf{Q}_l + \mathbf{q}_2, \beta} - c_{\mathbf{N}_l + \mathbf{Q}_l + \mathbf{q}_1, \alpha}^\dagger c_{\mathbf{N}_l + \mathbf{q}_2, \beta} \right. \\ \left. - c_{\mathbf{N}_l + \mathbf{q}_1, \alpha}^\dagger c_{\mathbf{N}_l + \mathbf{Q}_l + \mathbf{q}_2, \beta} \right) . \quad (\text{B1})$$

The label l can take values 1 or 2, allowing us to consider both the decoupled channels in the PG (associated with \mathbf{N}_1 and \mathbf{N}_2). It also labels the nesting vectors \mathbf{Q}_l associated with the two sets. α and β indicate spin indices, and \mathbf{q}_1 and \mathbf{q}_2 represent incoming and outgoing momenta in the scattering processes.

Because of the decoupling of the channel $l = 1$ and $l = 2$, we consider only the $l = 1$ channel for the rest of the calculations in this section. In order to simplify the Hamiltonian, we define new fermionic operators

$$\psi_{\mathbf{q}, \sigma} = \frac{1}{\sqrt{2}} (c_{\mathbf{N}_1 + \mathbf{q}, \sigma} + c_{\mathbf{N}_1 + \mathbf{Q}_1 - \mathbf{q}, \sigma}) , \quad \phi_{\mathbf{q}, \sigma} = \frac{1}{\sqrt{2}} (c_{\mathbf{N}_1 + \mathbf{q}, \sigma} - c_{\mathbf{N}_1 + \mathbf{Q}_1 - \mathbf{q}, \sigma}) , \quad (\text{B2})$$

The operator satisfy fermionic anticommutation relations. For convenience, we define new number operators for the sum and relative degrees of freedom:

$$s_{\mathbf{q}, \sigma} = \psi_{\mathbf{q}, \sigma}^\dagger \psi_{\mathbf{q}, \sigma} , \quad r_{\mathbf{q}, \sigma} = \phi_{\mathbf{q}, \sigma}^\dagger \phi_{\mathbf{q}, \sigma} . \quad (\text{B3})$$

We then have the following useful relation between the corresponding number operators $n = c^\dagger c$:

$$n_{\mathbf{N}_1 + \mathbf{q}, \sigma} + n_{\mathbf{N}_1 + \mathbf{Q}_1 - \mathbf{q}, \sigma} = s_{\mathbf{q}, \sigma} + r_{\mathbf{q}, \sigma} . \quad (\text{B4})$$

In terms of these new degrees of freedom, the auxiliary model Hamiltonian takes the form

$$\tilde{H} = -\frac{1}{2} W \sum_{\mathbf{q}, \sigma} r_{\mathbf{q}, \sigma} + W \sum_{\mathbf{q}_1, \mathbf{q}_2} r_{\mathbf{q}_1, \uparrow} r_{\mathbf{q}_2, \downarrow} + \sum_{\mathbf{q}_1, \mathbf{q}_2, \alpha, \beta} J^* \mathbf{S}_d \cdot \boldsymbol{\sigma}_{\alpha\beta} \phi_{\mathbf{q}_1, \alpha}^\dagger \phi_{\mathbf{q}_2, \beta} + \sum_{\mathbf{q}, \sigma} \varepsilon_{\mathbf{N}_1 + \mathbf{q}} (\psi_{\mathbf{q}, \sigma}^\dagger \phi_{\mathbf{q}, \sigma} + \phi_{\mathbf{q}, \sigma}^\dagger \psi_{\mathbf{q}, \sigma}) , \quad (\text{B5})$$

where we have considered a simplified form of the bath interaction (for the channel $l = 1$), taking into account the density-density correlations in k -space.

For bath interaction strength close to the critical value ($W \lesssim W_c$), the fixed point coupling value J^* is much smaller than W . In order to obtain the gapless excitations of the system arising from the presence of the impurity site, we integrate out the impurity dynamics via a Schrieffer-Wolff transformation. The perturbation term \mathcal{V} then consists of Hamiltonian terms that modify the impurity configuration,

$$\mathcal{V} = \sum_{\mathbf{q}, \sigma} \varepsilon_{\mathbf{N}_1 + \mathbf{q}} (\psi_{\mathbf{q}, \sigma}^\dagger \phi_{\mathbf{q}, \sigma} + \phi_{\mathbf{q}, \sigma}^\dagger \psi_{\mathbf{q}, \sigma}) + \sum_{\mathbf{q}_1, \mathbf{q}_2} J^* S_d^+ \phi_{\mathbf{q}_1, \downarrow}^\dagger \phi_{\mathbf{q}_2, \uparrow} + \text{h.c.} , \quad (\text{B6})$$

while the “non-interacting” Hamiltonian is

$$H_D = -\frac{1}{2} W \sum_{\mathbf{q}, \sigma} r_{\mathbf{q}, \sigma} + W \sum_{\mathbf{q}_1, \mathbf{q}_2} r_{\mathbf{q}_1, \uparrow} r_{\mathbf{q}_2, \downarrow} . \quad (\text{B7})$$

For the present Hamiltonian, the low-energy state is the one that minimises the bath interaction term $\tilde{H}_{\text{cbath-int}}$. High-energy states are obtained by applying, on the state $|L\rangle$, the excitation operator $\phi_{\mathbf{q}_1, \sigma}^\dagger \phi_{\mathbf{q}_2, \bar{\sigma}}$ or its hermitian conjugate.

The complete second-order renormalised Hamiltonian is

$$\Delta \tilde{H} = \sum_{\mathbf{q}, \sigma} \epsilon_{\mathbf{q}} r_{\mathbf{q}, \sigma} + \mathcal{U} \sum_{\mathbf{q}, \sigma} r_{\mathbf{q}\sigma} r_{\mathbf{q}\bar{\sigma}} + \mathcal{U} \sum_{\mathbf{q}_1 \neq \mathbf{q}_2, \sigma} \left[r_{\mathbf{q}_1, \sigma} r_{\mathbf{q}_2, \bar{\sigma}} + \phi_{\mathbf{q}_1, \bar{\sigma}}^\dagger \phi_{\mathbf{q}_1, \sigma}^\dagger \phi_{\mathbf{q}_2, \sigma} \phi_{\mathbf{q}_2, \bar{\sigma}} \right] . \quad (\text{B8})$$

where $\epsilon_{\mathbf{q}} = \text{sign}(\varepsilon_{\mathbf{N}_1 + \mathbf{q}}) \frac{\varepsilon_{\mathbf{N}_1 + \mathbf{q}}^2}{-W}$ and $\mathcal{U} = \frac{J^{*2}}{4W}$.